Nanorod Solar Cell

by

Bertha Tan

B.Eng. Material Science and Engineering
Nanyang Technological University, 2006

Submitted to the Department of Material Science and Engineering in Partial Fulfillment
of the Requirements for the Degree of

Master of Engineering in Material Science and Engineering
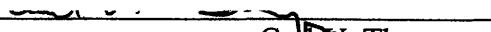at the
Massachusetts Institute of Technology

September 2007
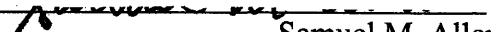
Signature of Author_____
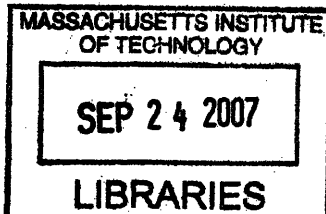Department of Materials Science and Engineering
July, 2007

Certified by_____
Carl V. Thompson
Professor of Materials Science and Engineering
Thesis Supervisor

Accepted by_____
Samuel M. Allen
POSCO Professor of Physical Metallurgy
Chair, Departmental Committee on Graduate Students

NANOROD SOLAR CELLS

by

BERTHA TAN

Submitted to the Department of Materials Science and Engineering
in partial fulfillment of the requirements for the Degree of Master of Engineering in
Materials Science and Engineering

Abstract

The crude oil supply crisis the world is facing today along with the disastrous global warming caused primarily as a result the green house gases, has heightened the need for an eco-friendly and renewable energy technology. Solar cells, with their ability to convert the free and gigantic energy supply of the sun into electricity, are one such attractive choice. In this thesis, a study of the use of new technologies for enhanced solar cell performance based on conversion efficiency is carried out by first understanding the mechanism of selected major solar cell types, followed by an analysis of external or internal factors that affect their performance. One new technology under investigation to boost solar cell efficiency is the introduction of nanorod/wire structures into existing designs. This report discusses this approach in detail, highlighting beneficial characteristics offered and also looking into the structure realization through advanced nanostructure processing techniques. Finally, having a complete technology background at hand, various potential markets for new solar cell technologies are examined.

Thesis Supervisor: Carl V. Thompson
Title: Professor of Material Science and Engineering

Acknowledgements

There are a number of people whom I would like to thank. This thesis would not have been possible without the help, support and guidance from them. First and foremost, I would like to thank Prof Carl V. Thompson for his time and patience in guiding and advising me. I would also like to thank Mr. Steven Boles for his efforts in discussing with me technical aspects of nanorod solar cells. In addition, I would also like to thank the administrative officers of the Singapore MIT Alliance (SMA) Programme and the Department of Material Science and Engineering (DSME) Office for the assistance rendered during the course of my studies. I would also like to thank my friends and classmates for their unwavering support. Last but not least, I would like to express my deepest gratitude to my family who has stood by me always.

Table of Contents

List of Figures

6

List of Tables

1. Introduction

The interest in green technologies was brought about by the dwindling supplies of crude oil as underground reserves are increasingly used up. This supply decline coupled with increasing demand for crude oil and the volatile Middle East situation has been a strong driving force for energy diversification into other alternatives such as nuclear, hydroelectricity, wind, geothermal, solar, etc.

Growing worldwide public sensitivity to the long-term importance of renewable energy sources has brought solar cells, one possible green technology candidate for addressing the energy crisis, into the market. In this technology, the gigantic energy supply from the sun, which is around $3 \times 10^{24} \; Joules/year$ (10,000 times more than the global population currently consumes) will be converted into electricity. Hence, covering 0.1% of the Earth's surface with solar cells of 10% efficiency, would satisfy our present needs.[1]

Photovoltaic (PV) or solar cell technology is currently enjoying substantial growth and investment. Governments in several develop countries have started to focus more attention and work on solar cell technology, as can be seen in many incentives, acts and national programs employed. While there are many possible options for PV materials and devices, the key performance metric is the cost per watt of PV-generated electricity. Hence, it makes efficiency as a crucial property of a solar cell.

Technological wise, the availability and robustness of various nanostructure processing methods through intensive and enormous studies have been done. This advancement has in some way triggered and hence opened an immense horizon of new solar cell designs which offer advantages over conventional designs or materials.

This report begins by briefly describing three major solar cell technologies, narrowed down to a specific solar cell structure of interest, which is nanorod solar cells, not only describing what it is, but also critically assessing their strong points, limitations and

10

methods of fabrication. Various markets around the globe are then examined. Having thus looked at the technology at hand and their potential market, a decision as whether to commercialize this particular solar cell design will be made. Last but not least, recommendations for future works will be delivered.

2. Nano-Rod/Wire Growth Techniques

Due to the advantages offered by nanorod/wire structures, as will be explained later, nanorods/wires have gained interest for incorporation and integration into devices. Solar cell technology is one application in which the offered advantages can be harvested. After growth techniques are discussed, the discussion will focus on fulfilling the criterion imposed by solar cell application. Fabrication of a nanorod/wire solar cell, be it silicon (Si) or material used in dye sensitize solar cell (DSC), requires creating dense arrays of well-oriented nanorods/wires. Nanowires are basically nanorods with higher aspect ratio. For the sole purpose of addressing simplification, nanorods are assumed to be the same as nanowires. Fabrication methods applicable to nanorod formation are also applicable to nanowires.

The overall fabrication process of nanorod structures consists of two steps, which are catalyst or seed deposition, followed by a growth process. Vapor-Liquid-Solid (VLS) is the common and robust method for growing silicon nanorods, whereas for DSC materials, VLS and solution based chemical synthesis are both applicable. VLS growth has the potential for rapid, low-cost deposition, scalability and compatibility with existing silicon thin film deposition techniques. Arrays of nanorods for both types of solar cells can be obtained either by templating or simply partial dewetting of thin metal catalyst film. However, it was found that the later method might result in nanorod size nonuniformity[2] due to randomness of the film breakup at reaction temperature.

A typical VLS process (Figure.1) starts with the dissolution of gaseous reactants into nanosized liquid droplets of a catalyst metal. Once the liquid droplet is supersaturated, nucleation and growth of single-crystalline rods will start to occur at the solid-liquid

interface. The one-dimensional growth is induced and dictated by the liquid droplets, whose sizes remain essentially unchanged during the entire process of wire growth, thus serving as a template to strictly limit the lateral growth of an individual rod and finally determine the diameter of nanorods grown. In general, the nanorod length can be controlled by simply modifying the growth time.
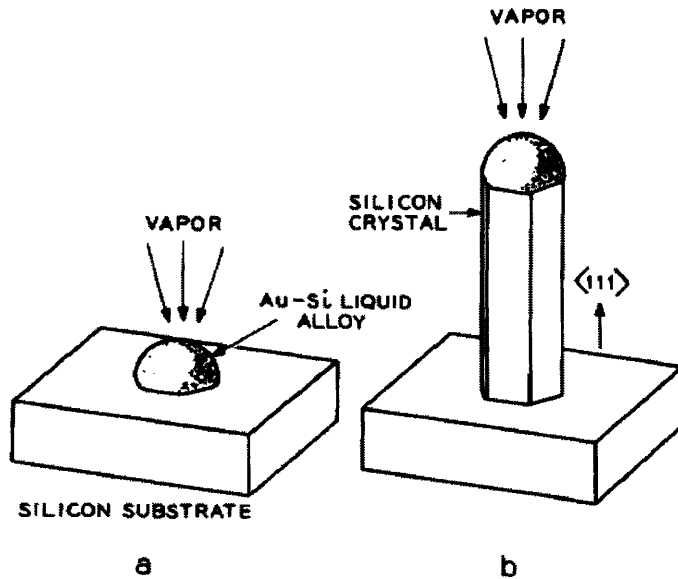
Figure 1. Schematic illustration of a silicon crystal grown with the VLS technique. (a) Initial condition with liquid droplet on substrate. (b) Growing crystal with liquid droplet at the tip.[3]

For a radial p-n junction nanorod solar cell, a dense array of well-oriented silicon nanorods, each with a radial p-n junction, as well as contacts to both the p- and n-type regions is required. The nanowires produced using the VLS approach with Au as a generally used metal catalyst are remarkable for their uniformity in diameter, which is usually on the order of 10 nm over a length scale of >1 μm. Furthermore, nanowire synthesis techniques can yield single-crystalline structures with a much lower density of line defects than is typically found in bulk materials. As a result, one-dimensional nanostructures often feature a mechanical strength, stiffness, and toughness approaching the theoretical limits of perfect crystals.[4]
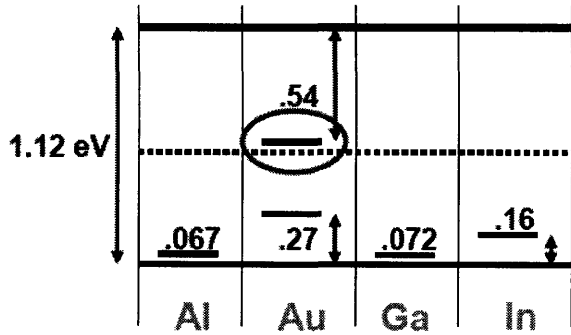
Figure 2. The relative location of trap state within the silicon bandgap for several dopants

Nevertheless, Au is known to form a deep-level trap state within the bandgap of silicon (Figure. 2) and hence can seriously degrade the electronic performance of silicon. After screening through some possible metal catalyst (e.g. Al[5], Ti[6] etc), silicon nanorods have been successfully grown by the VLS method using Indium (In) catalyst particles (Figure. 3), a step towards the fabrication of a nanorod solar cell. Even so, it was found that the uniformity of growth across a wafer from untemplated Indium was extremely poor. [2]
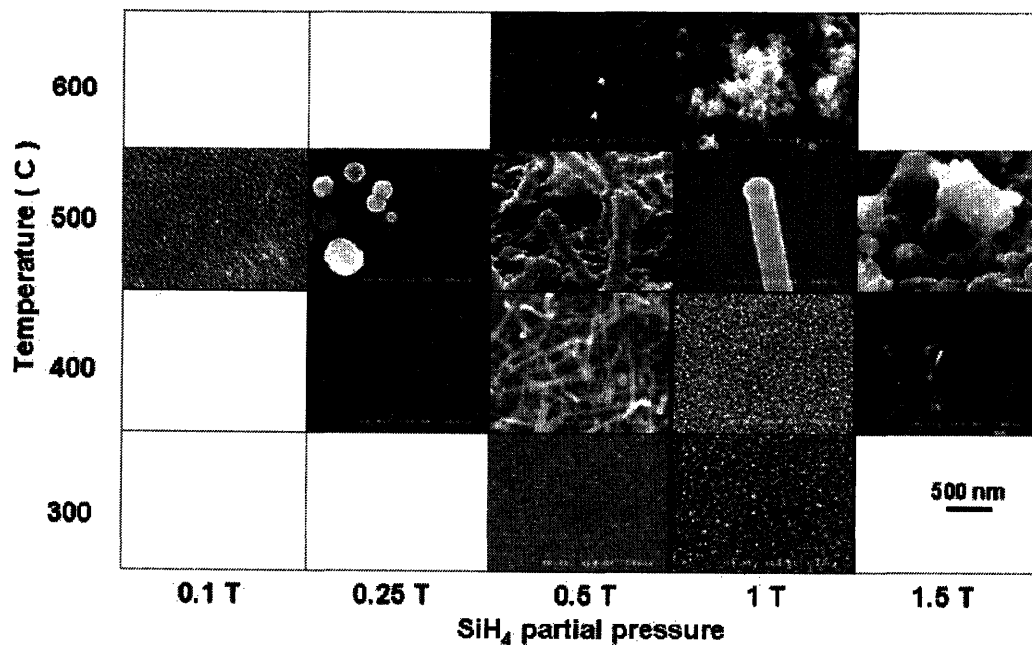
Figure 3. Partial phase diagram of growth of silicon nanorods from In catalyst particles as a function of pressure and temperature. In all cases the growth was achieved with silane (SiH$_4$) diluted to 5% concentration in Argon, with a flow rate of 100 sccm, for three hours. In most cases, catalyst particles were formed by the dewetting of a nominally 5nm thick evaporated film of In, but the results of growth were found to be relatively insensitive to catalyst layer thickness.[2]

In contrast with silicon nanorod growth, in DSCs, in which large bandgap semiconductor oxides are used (i.e. TiO_2, ZnO, etc), other growth process than VLS[7,8] will be needed, including seeded chemical synthesis, which is a low-temperature solution-based process. Dip coating and the usage of polyethylenimine (PEI) to enhance the aspect ratio of the rods produced has been studied by *Law et al* (Figure. 4).[9]
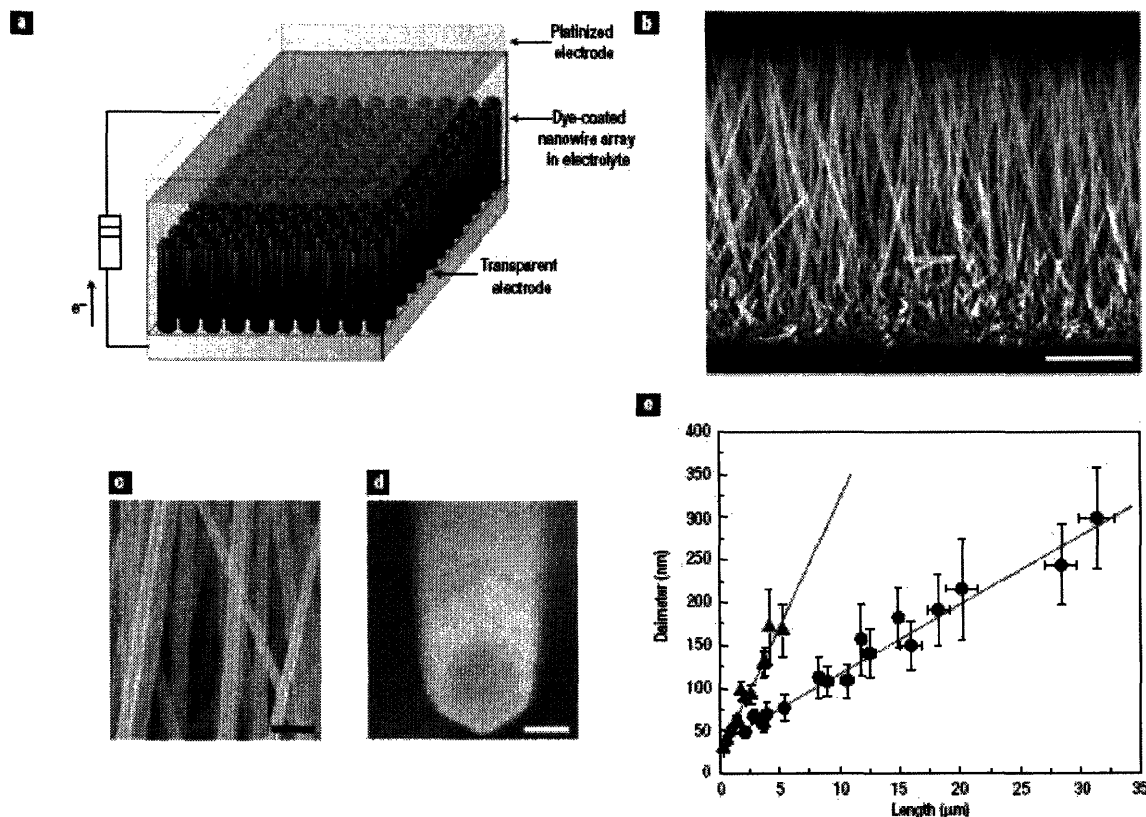
Figure 4. A nanowire dye-sensitized cell, based on a ZnO wire array. (a) Schematic diagram of the cell. Light is incident through the bottom electrode. (b) Typical scanning electron microscopy cross-section of a cleaved nanowire array on $F:SnO_2$ conductive glass (FTO). The wires are in direct contact with the substrate, with no intervening particle layer. Scale bar, 5 μm. (c) Magnified view of the oriented wires. In this array, wire length and diameter vary from 16 to 17 μm and 130 to 200 nm, respectively. Scale bar, 500 nm. (d) Typical top view of a single nanowire, showing its faceting, surface texture and a slight taper to its tip. Scale bar, 50 nm. (e) Wire length against diameter with (circles) and without (triangles) PEI added to the growth bath. Lines are least-squares fits to the data, and error bars represent one standard deviation.[9]

Since the rod/wire growth for both silicon and DSC cells is the continuation from metal catalyst or seeds deposited prior to the growth, templating methods will dictate the size, density, spatial distribution and crystal orientation of the resulting nanorods/wires. Approaches to templating of metal catalyst or seeds into an ordered manner include:

14

1. Electron Beam Lithography (EBL)[2] which is inherently a slow and high cost process. Mass production is hence tough to be realized, which is not desirable.

2. Anodized Aluminum Oxide (AAO)

   AAO is known to have ordered honeycomb nanopore arrays, perpendicular to the substrate. The diameter nanopores can be controlled from of order 10 nanometers to several hundred nanometers, and with density of several 10^9-10^{12} pores inch^{-2}.[10] In spite of the process robustness and availability of handy pores for templating purpose, it is generally difficult to obtain epitaxial growth of embedded material in the AAO nanopores, as an amorphous layer called the barrier layer exists at each nanopore bottom.

   There are mainly two approaches to remove the AAO barrier layer. One method is to separate the AAO membrane from the Al bulk by selective chemical etching of Al. The side of the AAO membrane with the barrier layer is then etched away to produce continuous pores. Putting this AAO membrane on a substrate, it can be used as shadow mask for evaporation to form nanodots arrays directly on a substrate.

   Another approach (Figure. 5) utilizes a thin aluminum film on a conductive substrate. The electrochemical formation of aluminum oxide stops as soon as all Al metal is consumed. The thinner AAO barrier formed on the conductive material is removed by chemical etching. In this case, the AAO membranes are fixed to the substrate. This is a big advantage compared with the first approach because it is possible to use the AAO nanopores as a template to control the growth direction of nanowires perpendicular to the substrate surface, even if the direction is not a preferred orientation for nanowire growth.
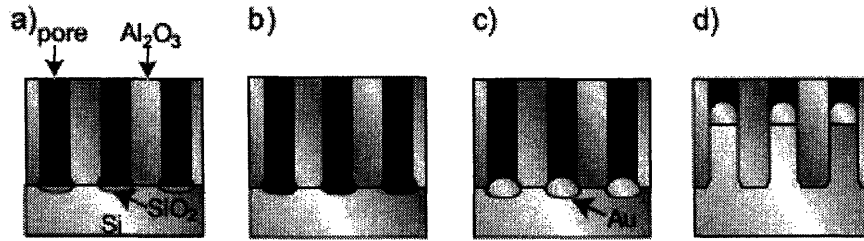
Figure 5. Schematic cross-sectional drawing of the growth of Si nanowires in AAO nanopores using Au nanoparticles as the catalyst. (a) After pre-annealing at 900 °C. (b) After HF etching to remove SiO_2. (c) Electroless Au deposition. (d) VLS growth of Si nanowires.[10]

Electroless or electrodeposition is used to form the array of metal catalyst, from which the nanorods are grown. In electroless deposition process using HF acid containing solution, direct contact between silicon and metal catalyst at each nanopore bottom is ensured and hence promoted epitaxially grown nanorod (Figure. 6). Crystalline quality of Si nanowires fabricated is better because the density of defects located at the interface between the original Si substrate and the nanowires was considerably reduced. This method is robust enough to control the diameter of nanowire grown from 60nm down to 10-20nm and higher density of nanowires ($69x10^9$ wires $inch^{-2}$).[10] With this method, desired crystal orientation growth perpendicular to the surface of the substrate is achievable. Furthermore, it also reduces the nonuniformity of the rods length as compared to other process.
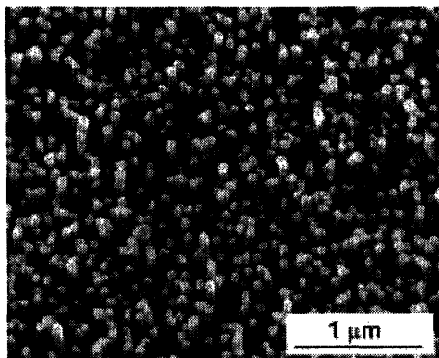
Figure 6. Side-view SEM image with 60° tilt of Si nanowires after selective etching of the AAO template by using phosphoric acid.[10]

16

3. Colloidal Seeding[11]

In this process, a thin polyelectrolyte layer is used to electrostatically attract gold colloids and immobilize them on the substrate. These gold colloids attached on the substrate will act as seeds for Si nanowire grown using the VLS-CVD method. The diameter of the colloids controls the nanowire diameter. Precise diameter control of nanowires grown by this method is limited only by the size distribution of the relatively monodispersed seed particles (colloids) used. The colloid solution concentration controls the density of growth. Spatial control was achieved by microcontact printing of the polyelectrolyte layer that confines wire growth to patterned regions (Figure. 7). Precise control over nanowire diameter, density and spatial distribution has made this process a versatile technique that facilitates incorporation of vertically aligned Si nanowires into more complex systems, enabling subsequent device integration.

Instead of employing the generally used precursor gas silane, $SiCl_4$ was used in this process. The gaseous byproduct, HCl, can be used to etch away the oxide layer on a Si surface, presenting a clean Si crystal surface for precipitation of Si from the binary liquid droplet, and thus enhancing epitaxially growth of nanowires.
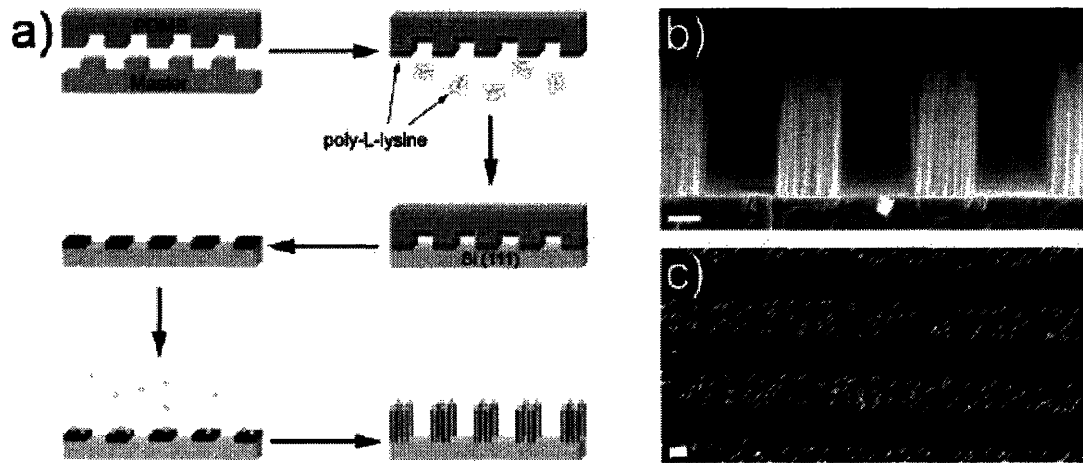
Figure 7. (a) Schematic of PDMS patterning of Au colloids. Briefly, a PDMS stamp is molded to the relief pattern of a photoresist master. After curing the polymer, the stamp is removed from the master and "inked" with a solution of poly-L-lysine. The stamp pattern is transferred to the Si (111) substrate, which is then immersed in the Au colloid solution. The colloid-patterned substrate is grown using conventional VLS-CVD synthesis, resulting in a corresponding pattern of SiNW arrays. (b) Cross-sectional SEM image of PDMS patterned SiNW growth, and (c) plane-view SEM image of the same. Scale bars are 1 μm.[11]

Colloidal seeding will be the most appealing process to produce dense array of nanorods, given the full control over the size, density and crystal orientation by simply manipulating the initial catalyst ($Au^{[11]}$). This process also gives a higher probability of having lower cost since it eliminates the need for using and dissolving a template. Furthermore, with the additional step of microcontact printing, the robustness of this process is even further enhanced. It is now possible to have full control of spatial distribution and grow nanorods in more complex systems. Since spatial distribution is not a major concern in nanorod solar cell designs discussed later, this additional step of microcontact printing which means additional cost can be eliminated.

On the other hand, a study done by *Kayes et al*[2] has shown extremely poor uniformity of growth across a wafer from untemplated In catalyst so that guided and templated growth is preferred. Hence, the combination of AAO templated and guided VLS growth processes will become the best choice to fabricate silicon nanorods if improvements in untemplated growth are not possible. On the contrary, metal oxide nanorods used in DSC will not be affected by the drawback caused by using Au as catalyst, hence no templating due to Indium catalyzed growth is necessary. However, AAO templates help in

18

controlling the density of the rods grown. Taken as a whole, this combined fabrication process is robust enough to meet the desired physical dimension for both silicon-based and dye-sensitized solar cells (Table. 1), by simply varying the AAO template pore size and thickness.

	Rod diameter	Length (μm)	Rod density	Special remark on growth condition
Desired for Si [23,26]	< 8 μm	~125	As high as possible	
Desired for DSC[24]	50nm	30	Pitch 70nm	
ZnO[7,8,33] VLS ZnO[9] Aqueous solution, seeded dip coating	(70-120) nm (130-200) nm	2-10 16-17	10^6-10^{10}/cm^2 35x10^9/cm^2	• Au thin film as catalyst. • Limited to aspect ratio of 20. With PEI, can be boosted to above 125. • Longest arrays of 20-25μm rods have surface area one fifth that of mesoporous film.
Guided AAO template [16]	(10-60) nm **Few-several hundred nm**	2	69x10^9/in^2 **10^9-10^{12}/in^2**	Experimented **Possible range**
Colloidal[15]	(40, 100) nm	3	0.1-1.8/μm^2	

Table 1. Summary of the nanords/wire physical dimensions obtainable based on several fabrication methods. The desired dimension for the silicon cell is based both on the simulation explained in the next chapter and the industrial constraints, whereas for the DSC it is based on the requirement for having the same surface area as the mesoporous structure generally used in a DSC.

3. Solar Cell Technology Description

3.1 Overview of Solar Cell

It is economically advantageous to be able to capture the energy that is freely available from sunlight and turn it into the valuable and strategically important asset that is electric power. Solar and photovoltaic cells are able to accomplish this goal by taking advantage of the fact that photons falling on a semiconductor material can create electron-hole pairs. With an interfacial built-in electric field at a junction between two materials, the electron-hole pair will be separated, and hence electrons flow and generate electricity.

19

A solar cell or photovoltaic cell is a device that converts light energy into electrical energy. Sometimes the term solar cell is reserved for devices intended specifically to capture energy from sunlight, while the term photovoltaic cell is used when the light source is unspecified. [12]
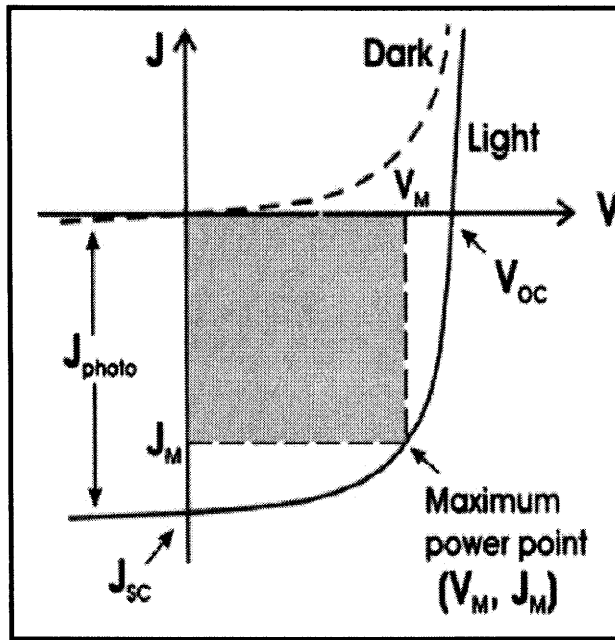
Figure 8. J-V characteristics of solar cell

An important feature that characterizes solar cell performance is conversion efficiency, which is defined by the equation $\eta = \dfrac{P_{out}}{P_{in}}$. Incident power $P_{in} = A \int\limits_{0}^{\infty} F(\lambda) \dfrac{hc}{\lambda} d\lambda$, describes the amount of energy absorbed from the sun, while power out $P_{out} = FF \times J_{sc} \times V_{oc}$ is the amount of electricity generated. Given the general formula above, it is clear that efficiency can be simply enhanced by either increasing the open circuit voltage (V_{oc}), short circuit current (J_{sc}) or the fill factor (FF).

The cell may be operated over a wide range of voltages and currents. By varying the load resistance from zero (a short circuit) to infinity (an open circuit), the point where the cell delivers maximum power and hence highest efficiency can be determined (Figure. 8). As power is the product of current and voltage, no power is produced at the short-circuit

current with no voltage, or at the open-circuit voltage with no current. Hence, the maximum power generated is expected to be found somewhere between these two points. In fact, the maximum power is generated at only one place on the power curve, at about the "knee" of the curve. This point represents the maximum efficiency of the solar device in converting sunlight into electricity.

A parameter known as the fill factor, $FF = \dfrac{J_m \times V_m}{J_{sc} \times V_{oc}}$, measures the "squareness" of the J-V curve and describes the degree to which the voltage at the maximum power point (V_m) matches V_{oc} and the current at the maximum power point (J_m) matches J_{sc}. FF is a measure of the ideality of a solar cell in operation. Hence, high valuea of all of the crucial parameters given is an required in order to achieve high overall efficiency

On the other hand, J_{sc}, here, is proportional to the external quantum efficiency (EQE), which refers to the ratio of the photocurrent generated (electrons delivered to the external circuit) per incident photon of a given wavelength. Hence a high EQE is desirable. Much research, involving different designs, materials and structures, has been done in order to push this conversion efficiency up.

In the classification done based on the structure and the materials used, solar cells are described as having four generations whose performance depend on their own distinct mechanisms. The first generation solar cell, silicon wafer-based solar cells, has reached a photon conversion efficiency of 24.7%, whereas second generation thin-film silicon devices have reached 12.7% and third generation nanocrystalline inorganic/polymer hybrids are at about 1.8-2.7%. The new fourth generation organic devices have reached approximately 5%.[13] (Figure. 9) shows the cost per watt of electricity generated based on this classification. As can be seen, people are working towards the lower cost-per-watt PV generated electricity by employing different designs and using engineered nanostructure solar cell.
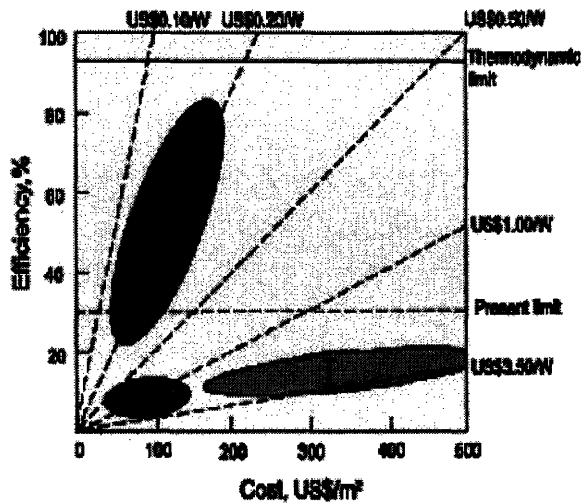
Figure 9. Cost per watt electricity generated from different generations of solar cell

Though there are other types of nanostructured solar cells that that have been proposed[14,15], three major and more established types of solar cell that will be thoroughly discussed in this report are:

1. Silicon based solar cells

2. Organic and hybrid (organic-inorganic) solar cells

3. Dye sensitized solar cells (DSC)

The correlation between the symbolic parameters given above (i.e. J_{sc} and V_{oc}) and the real mechanism involved in each type of solar cell will be analyzed.

3.2 Conventional Silicon-Based Solar Cells

The history of solar cells has so far been dominated by devices in which the junction is between inorganic solid-state materials. Over 95% of all the solar cells produced worldwide are composed of the semiconductor material silicon, be it crystalline or amorphous.[16] Historically, crystalline silicon has been used as the light-absorbing semiconductor in most solar cells, even though it is a relatively poor absorber of light and requires a considerable thickness (several hundred microns) of material. Nevertheless, it has proved convenient because it yields stable solar cells with good efficiencies (Table. 2).[16] In addition, silicon is abundantly available in nature and it has an established process technology developed from the huge knowledge base of the microelectronics industry.

22

Two types of crystalline silicon are used in the industry. The first is monocrystalline, produced by slicing wafers (up to 150mm diameter and 350μm thick) from a high-purity single crystal boule. The second is multicrystalline silicon (mc-Si), made by solidification of liquid silicon into blocks that are subsequently sawed into plates.

Unfortunately, Si-PV manufacturers use low-grade feedstock consisting of pot scrap, off-spec and remelt, much of this being rejected material from the microelectronics industry. The impurities present in the feedstock are carried over into the melt and into the grown crystal as dictated by segregation coefficients. Hence, in general, the PV-starting material has a high impurity content.

Defects are discontinuities in the periodic lattice, with associated dangling bonds. Like impurities, defects introduce bandgap states (energy levels in the bandgap). Due to the high impurity content mentioned above and the tendency of defects to interact with impurities to form precipitates, the properties of defects are very sensitive to impurities in the material. Hence, crystal defects always appear to have detrimental effects on the material (i.e. they cause recombination enhancement).[17]

The single-crystal Czochralski (Cz) ingots for PV are pulled at growth rates that can be many times faster than that of conventional growth for microelectronics. These fast cooling rates are accompanied by excessive thermal stresses that lead to the generation of defects. Consequently, the single-crystal material is expected to have high concentrations of quenched-in, nonequilibrium point defects.

As for mc-Si substrates, crystal structures of varying sizes are formed during solidification. These grains are typically a few millimeters to several centimeters in size, with dislocation as the dominant intra-grain defect. In addition, mc-Si substrates have a tendency to form localized clusters of defects which are networks of dislocations, stacking faults, and grain boundaries. Impurity precipitation occurs preferentially at these localized defect clusters (Figure. 10) rather than at grain boundaries and other isolated

defects.[17] Hence, having higher crystal defect densities inherited from the process, coupled with impurity precipitation, mc-Si cells are less efficient.
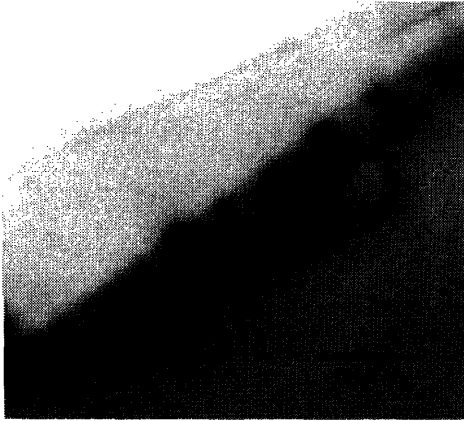
Figure 10. Transmission electron microscopy image of precipitates at a defect cluster[17]

Material	Level of efficiency in % Lab	Level of efficiency in % Production
Monocrystalline Silicon	approx. 24	14 to17
Polycrystalline Silicon	approx. 18	13 to15
Amorphous Silicon	approx. 13	5 to7

Table 2. General efficiencies of currently marketable silicon-based solar cells[16]

For crystalline silicon solar cells, a semiconductor homojunction is formed by diffusing phosphorus (n-type dopant) into the top surface of boron doped (p-type) silicon wafers. At the junction between the p and n doped regions, an internal electric field is built up which leads to the separation of the charge carriers that are generated due to light absorption. Screen-printed contacts are applied to the front and back of the cell, with the front contact pattern specially designed to allow maximum light exposure of the Si material with minimum electrical (resistive) losses in the cell (Figure. 11). A transparent anti-reflection film protects the cell and decreases reflective loss on the cell surface. Through metal contacts, an electric charge can be tapped. The cells are hermetically sealed under toughened, high transmission glass to produce highly reliable, weather-

resistant modules. Silicon cells are approximately 15 cm by 15 cm with a thickness of around 0.3 mm. The thickness of the n-type semiconductor layer approximately 2 μm.[16]

Rear Contact

Back surface field

Anti reflection coating

Front Contact

Texturing of front surface

E_C

E_g

E_V

h

E_F
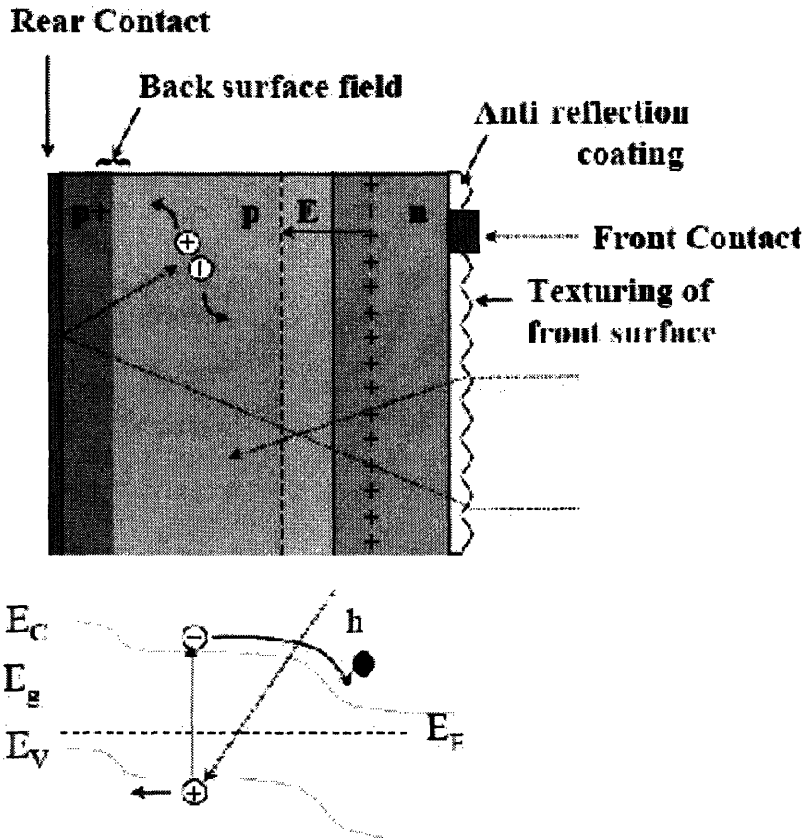
Figure 11. Schematic diagram of a typical solar cell structure (top) and the corresponding energy band diagram (bottom)[16]

3.3 Organic Solar Cell

Inorganic semiconductors are ideal for fabricating highly efficient solar cells, as they absorb a broad range of light and transport charge effectively, owing to their unique bandgap energy and high carrier mobility respectively. However, bulk inorganics require expensive processing that requires vacuum and high temperature process steps, limiting the cost-effectiveness of conventional inorganic solar cells. This high production cost has become the main motivation for intensive research into organic photovoltaic cells, since small-molecule and especially polymer semiconductors have the potential to be mass-produced and inexpensively processed into flexible, thin-film photovoltaics. Moreover, organic cells can be colored, which serves the need for robust design applications and aesthetic purposes.

Organic electronic materials are conjugated solids where both optical absorption and charge transport are dominated by partly delocalized π and π^* orbitals. Major differences between organic PV and inorganic semiconductors are:

- Photogenerated excitations (excitons) are strongly bound and do not spontaneously dissociate into charge pairs. Dissociation requires an input energy of ~100meW compared to a few meV for crystalline semiconductors

- Charge transport proceeds by hopping between localized states, rather than transport within a band, and mobilities are low

- The spectral range of optical absorption is relatively narrow compared to the solar spectrum

- Absorption coefficients are high (10^7 cm^{-1})

- Many materials are susceptible to degradation in the presence of oxygen or water

The first two features of organic solar cell are due to the fact that the intermolecular van der Waals forces in organic solids are weak as compared to bonds in inorganic crystals and much weaker than the intramolecular bonds. Hence, rather than forming bands, all electronic states are localized on single molecules. Additionally, the high degree of disorder present in many organic solids further renders carrier mobilities low.

3.3.1 Organic Solar Cell Development[18]

3.3.1.1 Homojunction

The simplest device structure is a layer of organic material sandwiched between two different conducting contacts, typically indium tin oxide (ITO) and a low work function metal such as Al, Ca or Mg. The work function difference provides an electric field, which drives separated charge carriers towards the respective contacts. However, this electric field is seldom sufficient to break up the photogenerated exciton. Instead, the exciton diffuses within the organic layer until it reaches a contact, where it may be broken up to supply separate charges, or recombine (Figure. 12).

26
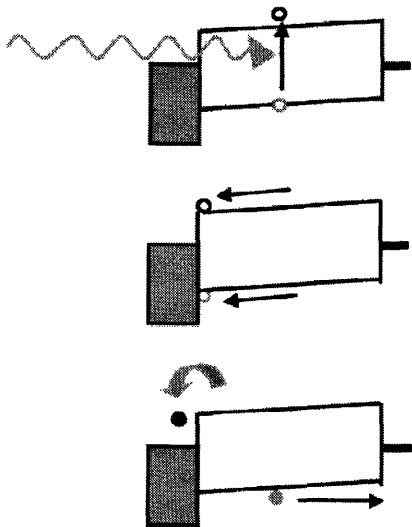
Figure 12. Schematic energy band diagram of a simple device consisting a single organic layer between two metal contacts[18]

Since exciton diffusion lengths are short, typically 1-10nm[18], exciton diffusion limits charge carrier generation in such devices. Photocarrier generation in this structure is therefore a function not only of bulk optical absorption, but also of available mechanism for exciton dissociation.

3.3.1.2 Heterojunction

Further development that has improved performance of organic PV devices is based on donor-acceptor heterojunctions (Figure. 13). As the name suggest, two different materials with different ionization potentials or electron affinities are used. The material with a greater electron affinity or ionization potential than the other is called the electron acceptor while the other is called the electron donor.
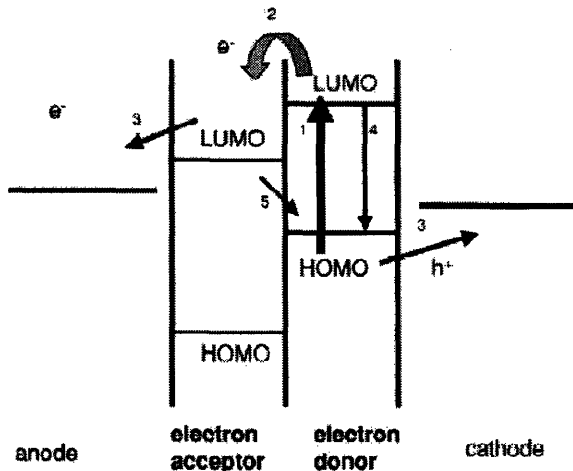
Figure 13. Schematic energy band diagram of a donor-acceptor heterojunction If both the excited state (LUMO) and ground state (HOMO) of the donor material lie at energies sufficiently higher than those of the acceptor material, it is energetically favorable for an exciton reaching the interface to dissociate, leaving a positive polaron on the acceptor and a negative polaron on the donor. For efficient photocurrent generation, charge separation (2) should compete successfully with recombination (4) after a photon absorption event (1), and transfer to contacts (3) should compete with interfacial recombination (5) [18]

These differences in electron affinity or ionization potential will result in electrostatic forces at the interface, hence createing an interfacial electric field. These local electric fields are strong and may break up photogenerated excitons, provided that the differences in potential energy are larger than the exciton binding energy.

Hence, previous inefficient charge separation due to the absence of strong local electric field, as seen in homojunction structures, is resolved by adopting this structure. However, the distance over which excitons need to travel before they encounter this local electric field at the interface might be greater than the exciton diffusion length. Therefore, this will render, once again, a non-optimum photocarrier generation condition.

3.3.1.3 Dispersed Heterojunction

A further revolutionary development in organic PVs was the introduction of dispersed heterojunctions (Figure. 14). An electron accepting and an electron donating material are blended together so that the length scale of the blend is similar to the exciton diffusion length. Hence with this numerous heterojunctions, wherever an exciton is photogenerated in either material, it is likely to diffuse within its diffusion length to an interface and break up.

28
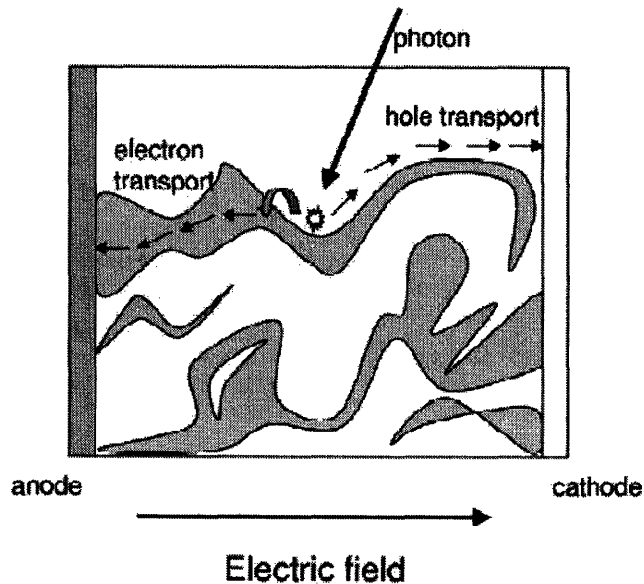
Figure 14. Schematic diagram of dispersed heterojunction cell[18]

When continuous paths exist in each material, from the interface to the respective electrodes, the separated charge carriers may travel to the contacts and deliver current to the external circuit. However, it is very difficult to control the process in order to achieve steady optimum blend morphology.

(Table. 3) shows that whilst organic solar cells produce quite respectable open-circuit voltages, the short-circuit photocurrent and fill factor are much lower than those available from inorganic devices. The lower photocurrent is due to poorer light absorption as well as photocurrent generation (charge separation) and transport; the fill factor is due to poor transport and recombination.

Material system	J_{sc} (mA cm^{-2})	V_{oc} (V)	Fill factor	Efficiency (%)	Peak QE, and wavelength (nm)	Reference
Doped pentacene heterojunction	7.7	0.90	0.66	4.5	–	[**15]
Doped pentacene homojunction	5.3	0.97	0.47	2.4	36% at 650 nm	[**14]
Cu phthalocyanine/ C60 bi-layer cell	13 (?)	0.53	0.52	3.6	18% at 620 nm 35% at 400 nm	[**17]
MDMO-PPV-PCBM	5.25	0.82	0.61	2.5	50% at 470 nm	[**18]
Dye sensitised solar cell with OMeTAD hole conductor	5	0.90	0.56	2.56	38% at 520 nm	[**21]
Amorphous silicon	19.4	0.887	0.74	12.7	~90%	http://www.pv.unsw.edu.au/eff
Monocrystalline silicon	42.2	0.706	0.83	24.7	>90%	http://www.pv.unsw.edu.au/eff

Table 3. Key performance characteristics, peak QE and absorption edge of several organic cells[18]

The absorption bandwidth in organic PV material depends on the material's degree of conjugation. Wider spectral sensitivity is achievable with highly conjugated dye molecules leaving the structure robust enough for optimum solar spectrum absorption. However, most conjugated solids absorb in the blue or green; absorption in the red or infrared is harder to achieve.

The efficiency of these devices is, however, limited by inefficient hopping charge transport. On top of inherently low carrier mobilities, electron transport is furthermore hindered by the presence of structural traps in the form of incomplete pathways in the percolation network. Therefore, higher efficiency requires improvements in absorption of red light, charge transport, and in material stability.

3.3.2 Hybrid (Organic-Inorganic) Solar Cell

For many conjugated polymers used in organic PV cells, electron mobilities are extremely low, typically below 10^{-4} $cm^2V^{-1}s^{-1}$, due to the presence of ubiquitous electron traps such as oxygen. For this reason, organic PV cells generally have relatively low efficiencies. Nevertheless, by introducing inorganic semiconductor materials with their superior characteristics, higher efficiency can be attained.

Energy levels of inorganic semiconductors naturally differ from those of organic semiconductors and are typically well aligned for charge transfer. With this staggered energy level (Figure. 15), charge transfer is favored between high electron affinity inorganic semiconductors and relatively low ionization potential organic molecules and polymers. This process can be remarkably fast in the case of organics that are chemically bound to nanocrystalline inorganics, as in dye-sensitized solar cell.
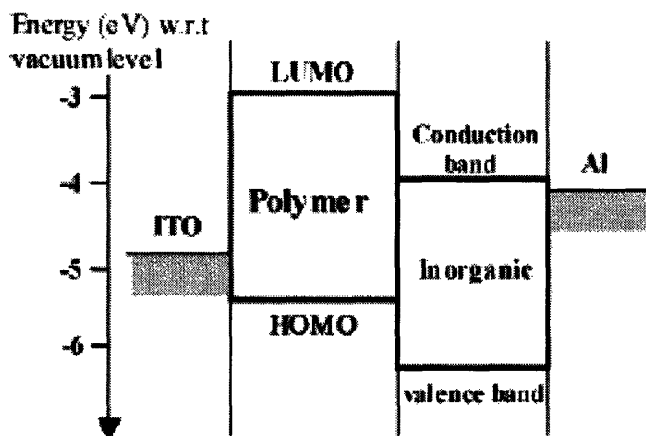
Figure 15. Staggered band gap arrangement for organic-inorganic heterojunction photovoltaic cell[19]

Inorganic semiconductors have high intrinsic carrier mobilities, which will improve the charge transport process. On the other hand, achievable hole mobilities in polymers far exceed electron mobilities. This discrepancy once again emphasizes the advantage of introducing inorganic semiconductor with the organic PV materials used. By doing so, benefits from both classes of material can be integrated.

Semiconductor nanocrystals (NC), have the combined advantageous characteristics of bulk inorganic materials, with the low-temperature solution based processability often being incorporated in hybrid devices. Due to the nanoscale nature of light absorption and photocurrent generation in solar energy conversion, the advent of methods for controlling these inorganic materials on the nanometer scale opens new opportunities for the development of future generations of solar cells. Colloidal processing of inorganic NCs is robust, and shares all the primary advantages of organics (scalable and controlled synthesis, an ability to be processed in solution and a decreased sensitivity to substitutional doping) while retaining the broadband absorption and superior transport properties of traditional PV semiconductors.

The light absorption in semiconducting polymers can be rather strong. However, it occurs over a discrete energy range covering only part of the solar spectrum. As such, blends should ideally incorporate materials with complementary absorption spectra, preferably

extending into the difficult to achieve near-infrared (NIR) range. As an additional design criterion, a clear energetic driving force for charge transfer must be present in this hybrid system.

Fortunately, spectral sensitivity of hybrid devices can be adjusted by material selection and quantum confinement effects. In order to optimize the overlap with solar emission, absorption spectra of hybrid devices can be tuned by altering the diameter of the inorganic nanorods produced. Advances in synthesis techniques allow control over nanocrystal sizes and shapes to optimize photovoltaic performance.[20,21] One-dimensional nanorods are preferred to quantum dots or sintered nanocrystals in solar energy conversion, because they naturally provide a direct path for electrical transport. In addition, the length of the nanorods can be adjusted to the device thickness required for optimal absorption of incident light.

A study done by *Huynh et al*[21] using CdSe nanorods with poly(3-hexylthiophene) (P3HT) in a hybrid solar cell has shown that by tuning the nanorod diameter, significant change in the absorption spectrum can be obtained. Flexible thin films of high density inorganic nanorods dispersed in P3HT (Figure. 16) have been successfully obtained using room-temperature solution-casting process.
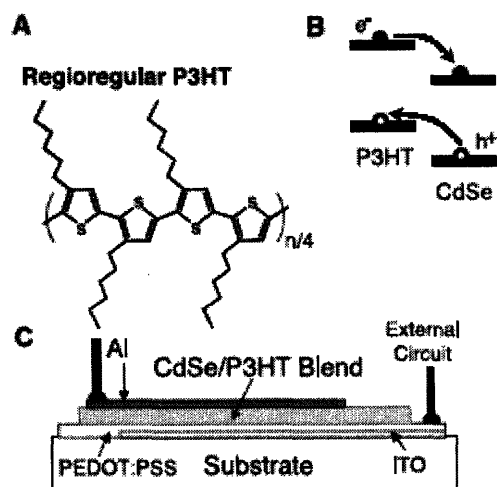
Figure 16. (A) The structure of regioregular P3HT. (B) The schematic energy level diagram forCdSe nanorods and P3HT showing the charge transfer of electrons to CdSe and holes to P3HT. (C) The device structure [21]

32

The solubility of inorganic nanorods with increasing aspect ratios has become an emerging issue for hybrid cells. However, a solvent mixture consisting of a good solvent and ligand for CdSe nanorods as well as for the polymer has been successfully developed to solve the issue. It is a mixture of pyridine and chloroform for the case of CdSe nanorods and P3HT hybrid cell.[21] CdSe is so far the most investigated material for hybrid PV cell. However, its usage has been restricted due to the high toxicity of cadmium.

In order for plastic nanorod devices to achieve power conversion efficiencies typical of conventional inorganic solar cells, it is necessary to reduce charge recombination, which decreases the EQE and the FF at solar light intensities. An increase in carrier mobilities would realize this by decreasing the carrier concentration within the device. Further enhancement of carrier mobilities can be accomplished by improving the nanocrystal-polymer interface to remove nanorod surface traps, aligning the nanorods perpendicular to the substrate, and further increasing their lengths.
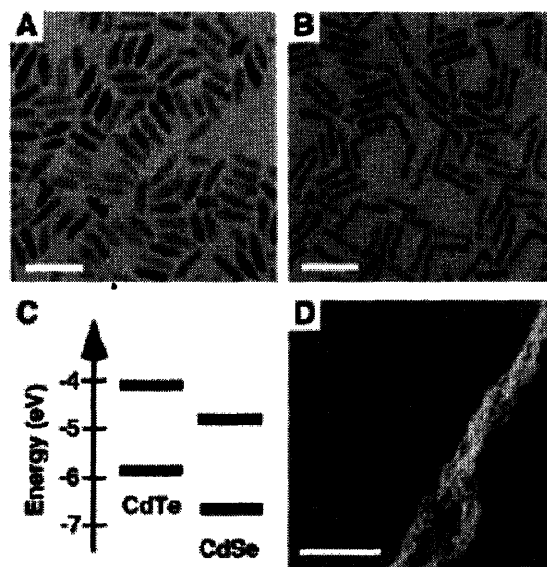
Figure 17. Transmission electron micrographs of (A) CdSe and (B) CdTe NCs used in this investigation. Scale bar, 40 nm. (C) An energy diagram of valence and conduction band levels for CdTe and CdSe illustrates the type II charge-transfer junction formed between the two materials. Employing the effective mass approximation, bulk energy levels were modified to account for quantum confinement. Valence band edges for CdSe and CdTe rods were calculated to be −4.79 eV and −4.12 eV, respectively. Conduction band edges for CdSe and CdTe rods were calculated to be −6.64 eV and −5.85 eV, respectively. (D) A typical spin-cast film of colloidal NCs imaged by scanning electron micrography is homogeneous and defect-free; the film edge of this È100-nm film is shown for contrast with the silicon substrate. Scale bar, 1 mm. [22]

33

The performance of hybrid devices, as discussed above is still ultimately limited by the low mobility and environmental sensitivity of their organic phase. Thus, *Gur et al*[22] have studied the possibility of using inorganic nanocrystals entirely for the device to eliminate the drawback of organics. The distinct carrier extraction trait of hybrid devices, which is not driven by built-in electric field created from a depletion region of susbtitutional dopants but rather primarily driven by directed diffusion, has also been observed in this all-inorganic PV cell. Directed diffusion by this staggered energy level necessary for charge extraction in this type of PV cell has also been observed in spin-cast thin film of CdTe and CdSe nanocrystals. (Figure. 17). Nevertheless, the overall efficiencies of either all organic, all inorganic or hybrid system are still below that of silicon-based PV cells.

3.4 Dye-Sensitized Solar Cell[23]

Dye sensitize solar cells (DSC), also referred to as Gratzel cells, consist of three important elements, namely:

- Organic dye that serves as a light absorber
- Nanocrystalline metal oxide that serves as electron transporter
- Liquid or solid state (i.e. organic polymer) electrolyte as hole transporter

Dye-sensitized solar cells are typically constructed from thick films of large bandgap semiconductor oxides, such as TiO_2, SnO_2, or ZnO nanoparticles that are sintered into a mesoporous network with a large internal surface area for the adsorption of light-harvesting dye molecules. Under illumination, excited states undergo rapid charge separation, followed by electrons injected into the nanocrystalline film and holes leaving the opposite side of the device by means of redox species in a liquid or solid-state electrolyte (Figure. 18). Subsequent discussion will be based on mesoscopic semiconductor oxide films, mainly TiO_2 and ZnO.

34

Grätzel, M. *Nature* 414, 2001.
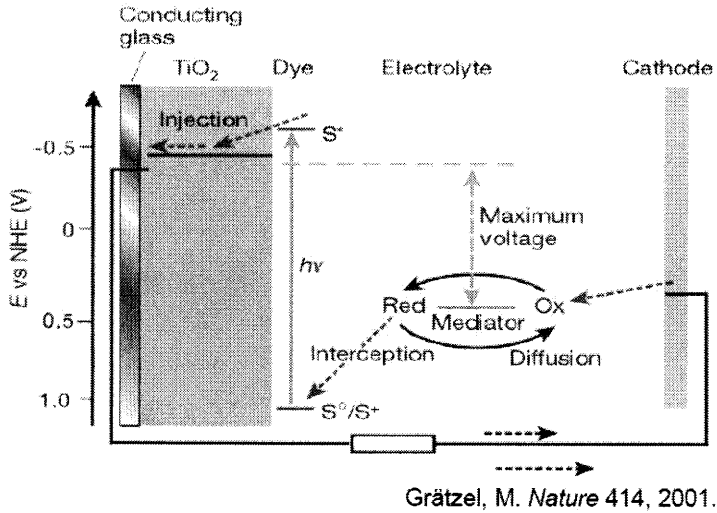
Figure 18. Schematic picture of dye-sensitized solar cell system[1]

The overall efficiency of this class of solar cell is still governed by the same formula in which high values of all the three crucial parameters; namely J_{sc}, V_{oc} and FF are desirable. The J_{sc} value will depend on how efficient the charge being generated from the absorbed photon and transported afterwards is. Since $J_{sc} \propto EQE$ as mentioned before, high EQE and carrier mobilities are still favored.

An additional step involved in DSCs, in contrast to other solar cell types, is electron injection from the excited dye through the interface into the metal oxide. This has then transformed the key parameter, which now can be expressed by the product $EQE(\lambda) = LHE(\lambda) \times \phi_{inj} \times \eta_{coll}$. Here LHE($\lambda$) is the light-harvesting efficiency for photons of wavelength λ, ϕ_{inj} is the quantum yield for electron injection from the excited sensitizer into the conduction band of the semiconductor oxide, and η_{coll} is the electron collection efficiency. Below, several stages that make up this additional step together with the parameters involved in each stage will be discussed.

3.4.1 Light Harvesting LHE(λ)

First of all, to achieve high power output, solar devices must take advantage of as much of the solar spectrum as possible as the photons absorbed by a solar cell directly impacts the power output. LHE(λ) will depend on the dye material used to absorb the solar

spectrum. The wider the spectral sensitivity range, the higher LHE(λ) will be. Hence, a dye that is able to efficiently absorb solar light across a broad range of wavelengths is desired. (Figure. 19) shows some widely used ruthenium based dyes in DSC. The performance of red ruthenium complexes, also identified as N3 or N719 was for a long time unmatched by any other dye.
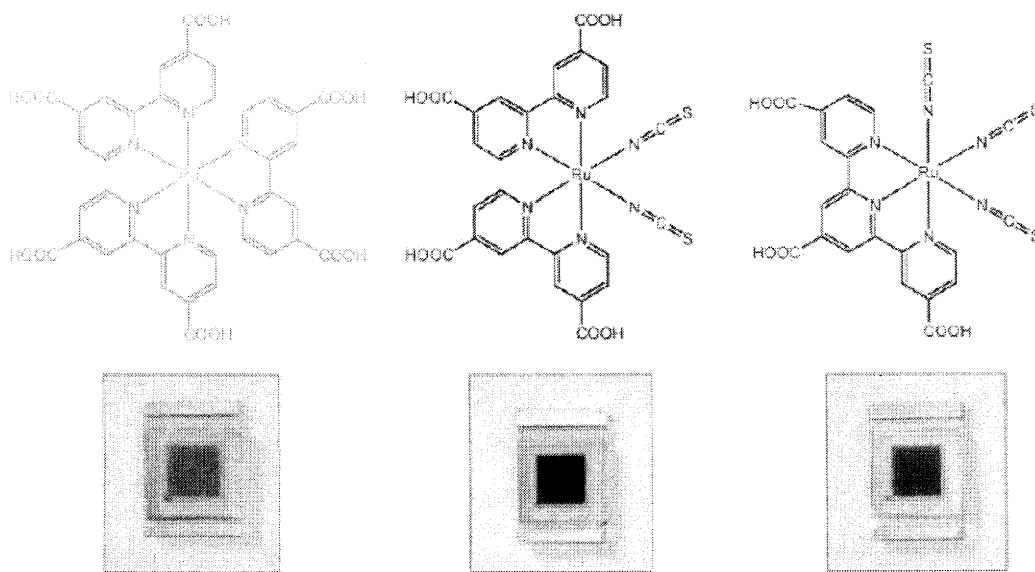
Figure 19. Structure of the ruthenium sensitizers RuL_3 (yellow) cis-$RuL_2(NCS)_2$ (red) and $RuL'(NCS)_3$ (green) where L = 2,2'-bipyridyl-4,4'-dicarboxylic acid and L' = 2,2',2''-terpyridyl-4,4',4''-tricarboxylic acid. The lower part of the picture shows nanocrystalline TiO_2 films loaded with a monolayer of the respective sensitizer. The film thickness is 5μm. [23]

Solar radiation includes invisible ultraviolet (UV) light, the visible spectrum of colors and the invisible infrared or IR spectrum whose percentage and wavelength can be seen in (Table. 4). Current dyes used mainly utilize the visible spectrum. However, due to the large percentage of IR spectrum in solar radiation, many attempts have been made to extend the absorption spectrum into the IR range to exploit solar spectrum more efficiently.[13]

	UV	Visible	IR
	(300 – 4045) nm		
Range (nm)		390-750	NIR (750-1400)
Percentage	3%	45%	52%

Table 4. Spectrum range and percentage of solar radiation partitions

3.4.2 Dynamics of Heterogeneous Electron Injection

Charge injection from the electronically excited sensitizer into the conduction band of the semiconductor is in competition with other radiative or radiationless deactivation channels. The deactivation of the electronically excited state of the sensitizer is generally very rapid. The rate constants for nonproductive channels can be summed as k_{deact}, with values in the range from 10^3 to 10^{10} s^{-1}.[23] Hence, to achieve a good quantum yield (ϕ_{inj}), the rate constant for charge injection should be at least two orders of magnitude higher than k_{deact}, which means injection rates in the picosecond range or below have to be attained.

Through a process called metal to ligand charge transfer (MLCT) (Figure. 20), the electron density shifts from metal employed in the dye (mostly Ruthenium) to the ligand, which should be the one that carries the attaching groups and the one from which very rapid electron injection into the semiconductor takes place. The dye's functional groups, such as carboxylate, hydroxyamate or phosphonate moieties, anchor the sensitizer to the oxide surface by forming a strong bond. On top of that, these groups also enhance the electronic coupling between the sensitizer's lowest unoccupied molecular orbital and the conduction band of the semiconductor. With molecularly engineered sensitizers such as those shown in (Figure. 19), the injection times in the pico- or femtosecond range can be achieved.
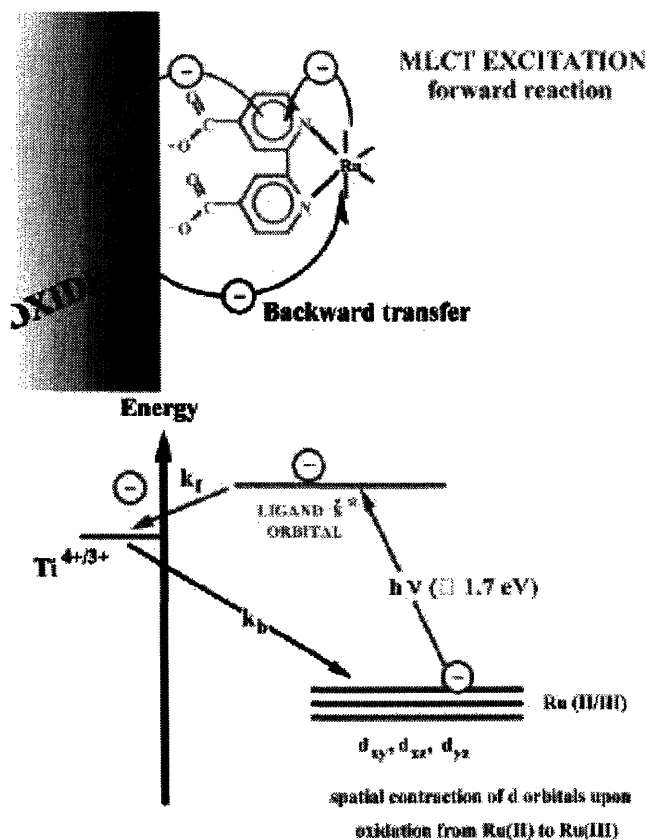
Figure 20. Interfacial electron transfer involving a ruthenium complex bound to the surface of TiO_2 via a carboxylated bipyridyl ligand. Orbital diagram for the forward electron injection (rate constant k_f) from the π^* orbital of the bipyridyl ligand into the empty t_{2g} orbitals forming the TiO_2 conduction band and the backward electron transfer from the conduction band of the oxide into the Ru(III) d orbitals. [23]

3.4.3 Light-Induced Charge Separation

As the next step, complete charge separation must be achieved. Competing with carrier injection is the thermodynamically favored back reaction with the oxidized sensitizer, characterized by a rate constant of k_b (Figure. 20). This reaction is undesirable because, instead of electrical current, it merely generates heat. Hence, sensitizer systems with high k_{inj} and low k_b are highly desirable.

While there is practically no depletion layer within the oxide due to the small size of the particles and their low doping level, a surface field is established spontaneously by proton transfer from the carboxylic acid groups of the ruthenium complex to the oxide surface, producing a charged dipole layer. This local potential gradient from the negatively charged sensitizer to the positively charged oxide drives the injection in the desired

38

direction. The same field also inhibits the electrons from exiting the solid after injection has taken place, and thus further inhibits charge recombination.

In the N-719 ruthenium sensitizer shown above, the forward injection is an extremely rapid process occurring in the femtosecond time domain. By contrast, the back reaction of the electrons with the oxidized ruthenium complex is one to two orders of magnitude smaller. [23]

3.4.4 Charge-Carrier Collection

Apart from recapture by the oxidized dye, the electrons can be lost to the electrolyte by reaction with the oxidized sensitizer from of the redox mediator, e.g., triiodide ions: (Figure. 21) illustrates the injection and recombination processes. The efficient interception of recombination by the electron donor, e.g., iodide, is thus crucial for obtaining good collection yields and a high cycle life of the sensitizer.
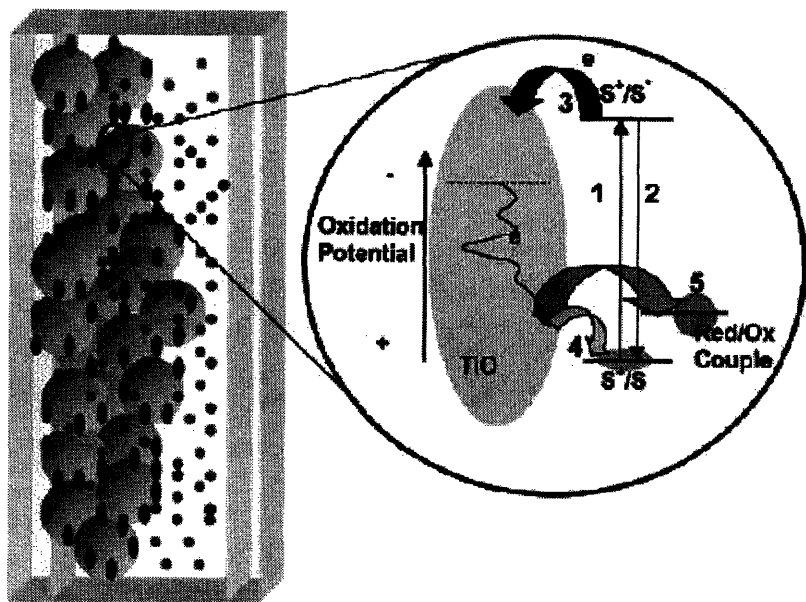
Figure 21. Photoinduced processes occurring during photovoltaic energy conversion at the surface of the nanocrystalline titania films: (1) sensitizer (S) excitation by light; (2) radiative and nonradiative deactivation of the sensitizer; (3) electron injection in the conduction band, followed by electron trapping and diffusion to the particle surface; (4) recapture of the conduction band electron by the oxidized sensitizer (S$^+$); (5) recapture of the conduction band electrons by the oxidized form of the redox couple regenerating the sensitizer and transporting the positive charge to the counter electrode. Gray spheres: titania nanoparticles. Small elongated dots: sensitizer. Small round dots: oxidized and reduced forms of the redox couple. [23]

In the case of N-719 mentioned before, time-resolved laser experiments have shown the interception to take place with a rate constant of about 10^5-10^7 s^{-1} at the iodide concentrations that are typically applied in solar cells. This is more than a hundred times faster than the recombination rate and $>10^8$ times faster than the intrinsic lifetime of the oxidized sensitizer in the electrolyte in the absence of iodide. [23]

Improved conversion efficiency in this class of solar cell can be obtained by maximizing solar absorption (extending the spectral sensitivity of the dye used into the NIR region), suppressing any recombination mechanisms and enhancing carrier diffusivity or mobility.

3.5 Technological Advantages

Advantages offered by harnessing nanorod structures were only discussed for silicon based solar cells and DSCs. Having discussed different cell mechanisms, it can be understood that hybrid cells operate in ways that are quite similar to DSCs and have relatively lower efficiency. Thus, they are of minor interest.

3.5.1 Radial p-n Junction Nanorods Solar Cell[24]

Inexpensive semiconductors that serve as light absorber materials for use in photovoltaic applications generally have either a high level of impurities or high defect densities, resulting in low minority carrier diffusion lengths, than materials used in microelectronics. Low-cost metallurgical silicon feedstock has impurity concentrations $>10^{15}$cm^{-3}, which corresponds to a minority diffusion length, $L_n< 8\mu m$.[25,26] Use of low-diffusion-length materials as the absorbing base in conventional planar p-n junction solar cell geometries results in devices having carrier collection limited by minority carrier diffusion in the base region. Increasing the thickness of the base in such a cell (so as to increase the number of excitons generated) will have no effect on the device efficiency, as excitons generated at a distance greater than the minority carrier diffusion length from the built in electric field will not contribute to the external current (Figure. 22).

40
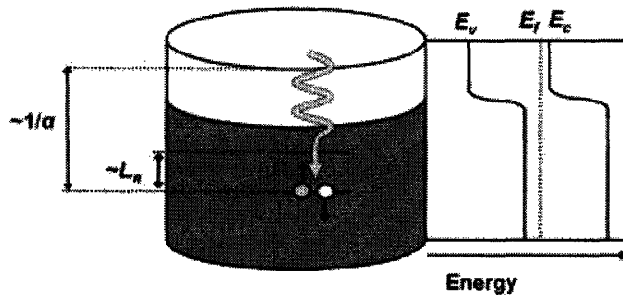
Figure 22. A conventional planar solar cell is a p-n junction device. Light penetration into the cell is characterized by the optical thickness of the material, while the mean free path of generated minority carriers is given by their diffusion length. In the case shown, light penetrates deep into the cell, but the electron diffusion length is too short to allow for the collection of all light-generated carriers. (Right) [24]

Silicon devices efficiently absorb and convert solar energy up to about 1,050 nm, covering approximately 75% of the total photon flux from the sun.[13] Having relatively wide spectrum sensitivity, it is a waste to not have optimum light absorption just because the thickness of the cell is limited by low carrier diffusion lengths.

Radial p-n junction nanorod cells provide a potential solution to this problem. This structure allows the separation for the requirements of light absorption and carrier extraction in two orthogonal directions. The cell can be thick in one dimension for optimal light absorption, while thin in another, for optimal carrier collection (Figure. 23).
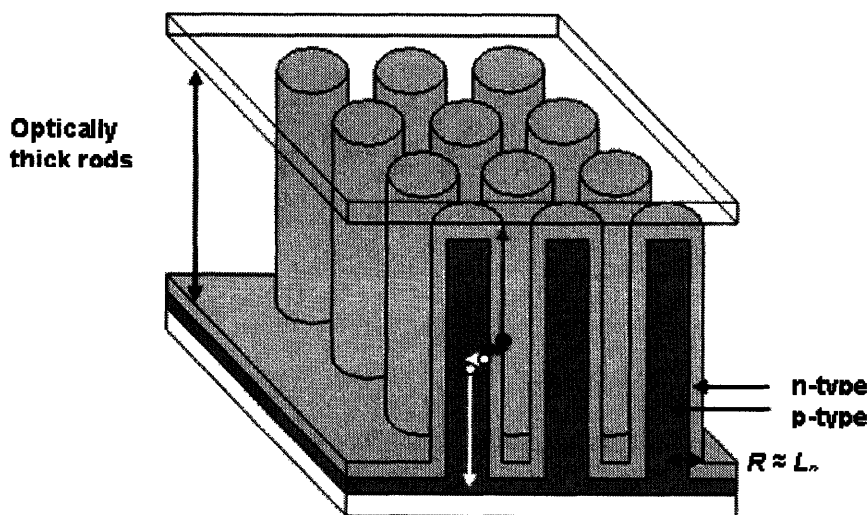
Figure 23. Schematic and cross-section picture of the radial p-n junction nanorod cell. Light is incident on the top surface. The light grey area is n-type, the dark grey area is p-type[26]

41

Modeling was done by *Kayes et al*[24] to obtain a quantitative comparison between the performance of the radial p-n junction nanorod geometry and the conventional planar p-n junction cell geometry. The modeling indicates that the design of the radial p-n junction nanorod device should provide large improvements in efficiency relative to a conventional planar geometry p-n junction solar cell, provided that two conditions are satisfied:

1. In planar solar cell made from the same absorber material whose diffusion length of minority carriers is taken as small compared to the optical absorption distance, so that the extraction efficiency becomes low

2. The rate of carrier recombination in the depletion region must not be too large (for silicon this means that the carrier lifetimes in the depletion region must be longer than 10 ns).

If only condition (1) is satisfied, the modeling indicates that the radial cell design will offer only modest improvements in efficiency relative to a conventional planar cell design. The model for the radial p-n junction nanorod solar cell was constructed by extending the analysis of the planar cell geometry to a cylindrical geometry. The p-n junction in the nanorod was assumed to be abrupt, and the depletion approximation was assumed to be valid. The emitter layer (nanorod shell) was assumed to be n-type, while the base (nanorod core) was assumed to be p-type.

The analysis considered purely inorganic homojunction and heterojunction devices with delocalized carriers and included the effects of free-carrier recombination, recombination at the junction, and surface recombination. Recombination was assumed to be purely due to the Shockley–Read–Hall recombination from a single-trap level at midgap; other recombination processes, such as Auger recombination, were neglected. Surface recombination effects were, however, included due to the enormous surface area created by adopting nanorod structure as compared to planar design.

To simplify the analysis and to allow for analytic solutions, the transport of generated excitons was taken to be purely radial. Although individual rods may have a high

resistivity, the voltage (IR product) drop in a nanorod can still be very low because of the very small current that will pass through each rod. Given a resistivity of ~10^{-2} Ω cm (appropriate for Si with doping 10^{18} cm^{-3}),[24] a rod length of ~100 μm, and a current density of ~0.05 A cm^{-2}, the IR drop in a rod due to series resistance is ~10^{-5} V. Hence, the exterior of the rod can be assumed to be an equipotential surface relative to the core of the rod. The total photogenerated carrier flux was calculated by an integration that is equivalent to summing up the contributions at each value of z at a given bias, and the dark current was calculated for the entire junction area neglecting the ends.

The approximation of one-dimensional carrier transport is valid when the variation in carrier concentration in the z direction occurs over a much longer length scale than that in the r direction (Figure. 24). This is an appropriate assumption for a radial p-n junction nanorod in a material that is collection limited, that is, one with an optical thickness much greater than the diffusion length of minority carriers. In this case, the variation in carrier concentration in the axial direction is primarily due to light absorption and occurs over a large distance relative to the variation in carrier concentration in the radial direction, which occurs due to diffusion and drift resulting from the potential drop at the p-n junction interface.

The light-generated current density in the depletion region (J_g^{dep}) was calculated by assuming that all absorbed incident light produced collected carriers. The recombination current density for the entire depletion region was calculated by multiplying the maximum recombination rate by a small volume centered about this maximum recombination point, which might lie in the p-type or n-type material.

Combining all the expressions for current density produced the following expression for the J-V behavior of the device is

$$J = (J_0^p + J_0^n)(e^{qV/kT} - 1) - J_l^p - J_l^n - J_g^{dep,p}(V) - J_g^{dep,n}(V) + J_r^{dep}(V),$$

where

J_0^p, J_0^n are the dark current densities in the p- and n- regions

J_l^p, J_l^n are the light generated current densities in the p- and n- quasi-neutral regions

$J_g^{dep,p}$, $J_g^{dep,n}$ are the light generated current densities in the p- and n- depletion regions

J_r^{dep} isthe recombination current density in depletion region

Surface recombination is incorporated into J_l^n.

The current density (J) was calculated at each value of forward bias (V) and at each wavelength, and the results were numerically integrated over wavelength to obtain a value for the total current-density versus voltage (J-V) curve. The the open-circuit voltage, short-circuit current density, fill factor, and efficiency were calculated based on this curve.

Two regimes/cases are treated here:

1. Constant trap density through the material, and thus the minority carrier lifetimes in the quasi-neutral region and in the depletion region were coupled

2. Trap density in the quasi-neutral region assumed to be independent of the trap density in the depletion region. In the simulation, the trap density in the depletion region was held fixed at 10^{14} cm^{-3}. This set of conditions simulated the situation in which the impurity profile was not constant throughout the sample. This case led to quasi-neutral region recombination being the dominant recombination mechanism.

The behavior of the cells was first investigated as a function of doping levels in the emitter and base, i.e. the emitter thickness and nanorod radius. At a given value of the minority-electron diffusion length, nanorod cells favored high doping. At a fixed trap density, increasing the doping decreases the mobility and hence decreases the diffusion length. On the other hand, increasing the doping level increases the built-in voltage. The detrimental effects of a low diffusion length are partially overcome by the nanorod geometry.

44

Doping concentrations for silicon semiconductors may range anywhere from 10^{13} cm^{-3} to 10^{18} cm^{-3}. A doping concentration above about 10^{18} cm^{-3} is considered to be degenerate at room temperature.[27] For silicon in this simulation, the maximum doping level was limited by the need to have a non-degenerate material, the recombination of which is not dominated by Auger processes. Hence, it is on the order of 10^{18}cm^{-3} and was not set to a higher value.

Hence an n^+ / p^+ structure was assumed, with the top layer (in case of the planar cell) or the external shell (in case of a nanorod cell) being n$^+$. d_1 (Figure. 24) was further set equal to the minimum value required to achieve a built in voltage V$_{bi}$. This corresponds to a value of $\sim 1 \times 10^{-6}$ cm for the doping concentration mentioned above.
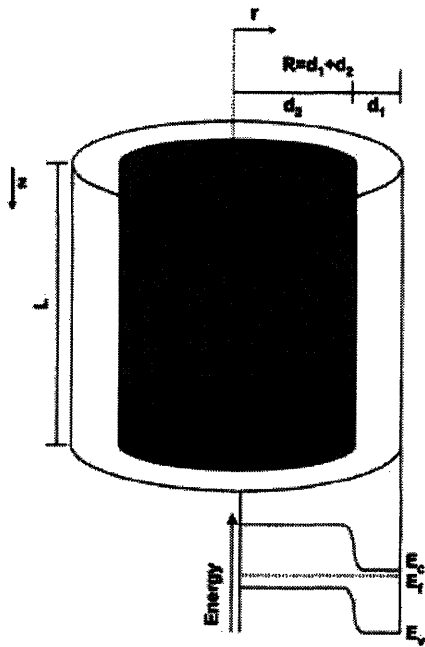
Figure 24. Schematic diagram of a single rod from the radial p-n junction nanorod cell, and its corresponding energy band diagram. Light is incident on the top surface..[24]

Further insight into the performance differences between the two cell geometries (Figure. 22, 24) were obtained by evaluating the simulated efficiency, V$_{oc}$, and J$_{sc}$, versus L and R for radial p-n junction nanorod cells. From (Figure. 25), it can be seen that J$_{sc}$ increased with increasing rod length, plateauing when the length of the rod became much greater than the optical thickness of the material. Also, J$_{sc}$ was essentially independent of rod

radius, provided that the radius was less than electron diffusion length L_n. The value of J_{sc} decreased steeply for $R > L_n$. J_{sc} was found to be essentially independent of trap density in the depletion region.

On the other hand, the open-circuit voltage (V_{oc}) decreased with increasing rod length as the junction area increased, and increased with increasing rod radius (Figure. 26). The extent to which V_{oc} decreased with increasing rod length depended strongly on the trap density in the depletion region: as the trap density became high ($> \sim 3 \times 10^{15}$ cm^{-3} for Si), in the depletion region, V_{oc} declined rapidly. The trap density in the quasi-neutral regions, on the other hand, had relatively less effect on V_{oc}.
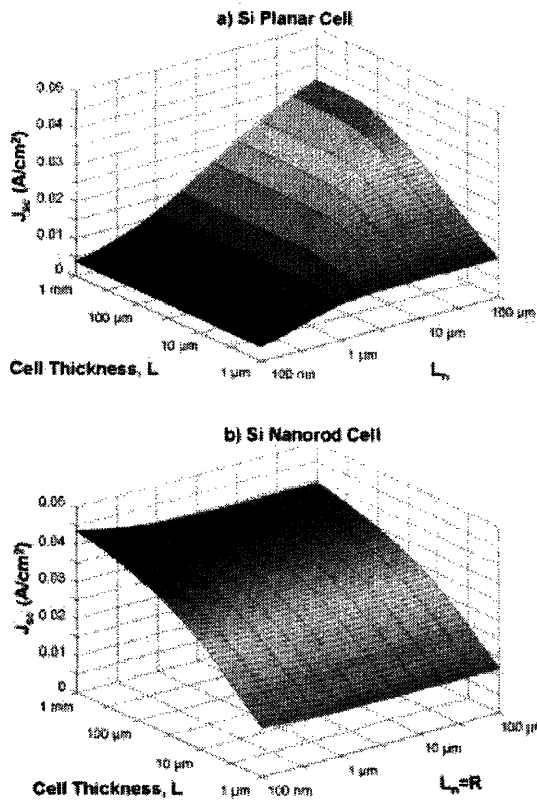
Figure 25. Short-circuit current density J_{sc} vs cell thickness L and minority-electron diffusion length L_n for (a) a conventional planar p-n junction silicon cell and (b) a radial p-n junction nanorod silicon cell. [24]
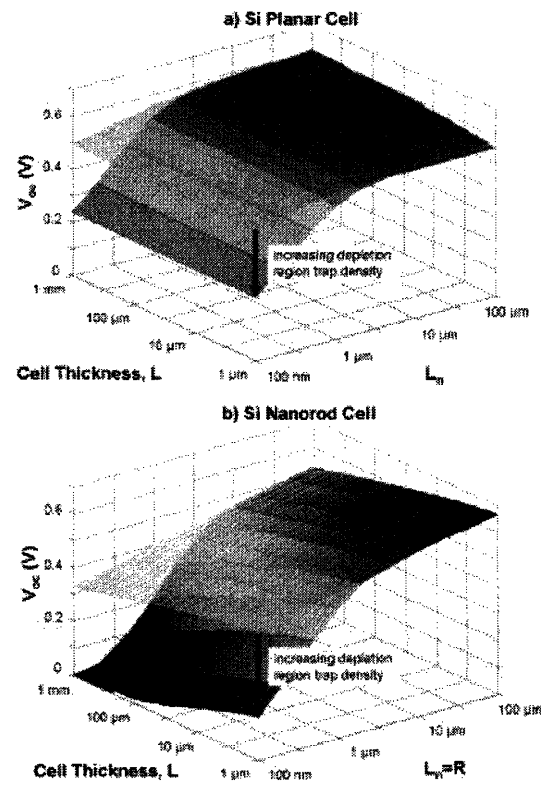
Figure 26. Open-circuit voltage V_{oc} vs cell thickness L and minority-electron diffusion length L_n for (a) a conventional planar p-n junction silicon cell and (b) a radial p-n junction nanorod silicon cell. In both cases the top surface shown in the plot has a depletion-region trap density fixed at 10^{14} cm^{-3}, while the bottom surface has a depletion-region trap density equal to the trap density in the quasi-neutral region, at each value of L_n. [24]

46

Because carriers can travel approximately one diffusion length through a quasi-neutral region before recombining, making the rod radius approximately equal to the minority-electron diffusion length allows carriers to traverse the cell even if the diffusion length is low, provided that the trap density is relatively low in the depletion region. The higher the doping concentration, the higher the built in electric field and the smaller the depletion width will be. Due to this higher driving force and smaller distance over which carriers need to travel, carrier collection becomes more efficient. This has further emphasized once again the benefit of radial p-n junction nanorod cells in having high doping levels to produce high cell efficiencies. Hence, the optimal rod dimensions are obtained when the rod has a radius approximately equal to L_n and a length that is comparable to the optical thickness of material used. This optimum length dimension was determined by the specific trade-off between the increase in J_{sc} and the decrease in V_{oc} with length.
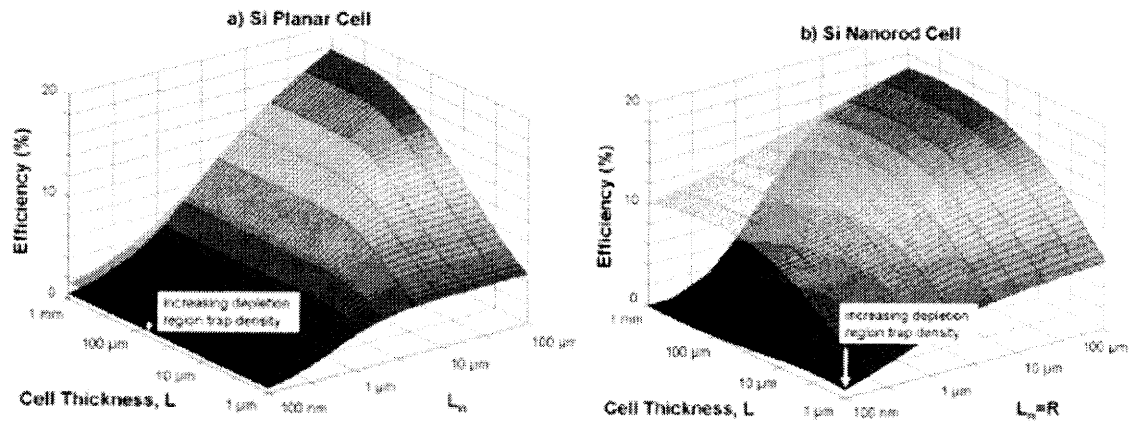
Figure 27. Efficiency vs cell thickness L and minority-electron diffusion length L_n for (a) a conventional planar p-n junction silicon cell and (b) a radial p-n junction nanorod silicon cell. In both cases the top surface shown in the plot has a depletion-region trap density fixed at 10^{14} cm^{-3}, while the bottom surface has a depletion-region trap density equal to the trap density in the quasi-neutral region, at each value of L_n. In the radial p-n junction nanorod case, the cell radius R is set equal to L_n, a condition that was found to be near optimal.[24]

L_n	N_r (cm^{-3})	η_{max} (planar)	η_{max} (radial)	Efficiency gain factor ($\eta_{radial}/\eta_{planar}$)
100nm	Quasi-neutral=7x10^{18}; Depletion=10^{14}	1.5%	11%	7.33
	Quasi-neutral=Depletion=7x10^{18}	0.5%	1%	2
1μm	Quasi-neutral=7x10^{16}; Depletion=10^{14}	5%	13%	2.6
	Quasi-neutral=Depletion=7x10^{16}	4%	7%	1.75

Table 5. Cell efficiency obtained by combining both simulated data on J_{sc} and V_{oc} for the two selected cases. L_n was obtained according to the trap density in the quasi-neutral region. As trap density increases, the minority carrier diffusion length decreases $L_n \propto \dfrac{1}{\sqrt{N_r}}$.

In summary, the radial p-n junction nanorod geometry has the potential to produce significant improvements in efficiencies of cells (Figure. 27) made from materials whose diffusion lengths are low relative to their optical thickness (diffusion length at least two orders of magnitude less than the optical thickness). In silicon with very low diffusion lengths (L_n=100 nm corresponds to N_r=7x10^{18}cm^{-3}), extremely large efficiency gains (~7 times those efficiency in planar geometry) are possible by exploiting the radial p-n junction nanorod geometry (Table. 5), with a crucial conditions of relatively low trap density in the depletion region. This increase is explained by the greatly enhanced carrier collection that is possible in the radial p-n junction nanorod cell.

Other than defects and impurities, dopants might also be considered as one source of traps, as they also form shallow trap states within the silicon bandgap. These high-density shallow traps might substantially affect the carrier lifetime. Hence, considering dopants as one source of traps, a minority diffusion length of ~100 nm is possible. This corresponds to an upper bound limit on the doping concentration of ~10^{18}cm^{-3}, before it turns degenerate. Hence, the condition of low minority carrier diffusion length simulated in the model is in fact closely related to the real condition. However, the extent to how high-density shallow traps influence the simulated results is not obvious, as the simulation only consider recombination from a single-trap level at midgap.

Au being a source of this midgap trap level is hence not considered a suitable metal catalyst for silicon nanowire growth. Although Au has a relatively low solubility in the

growing nanorod (segregation coefficient 2.5×10^{-5}), this nonetheless implies that Au concentrations of $\sim 10^{18} cm^{-3}$ will be present in nanorods.[2] This can create a high enough trap density to seriously degrade the electronic performance of silicon. Indium, despite of its higher segregation coefficient (4×10^{-4}), is considered as one possible substitute for Au since it only forms shallow acceptor states within the silicon bandgap.

Assuming that the surface state between silicon and its oxide has the same effect as traps in the depletion region, the depletion region trap density might be modeled by using the surface state density value of $2.5 \times 10^{11} eV^{-1} cm^{-2}$ for single crystals.[28] Integrating this value over the depletion region with a nanorod radius of 100 nm and length of 125 μm will result in a surface state density (i.e. depletion region trap density) on the order 10^{12} cm^{-3}. The maximum depletion region is taken to be $\sim$10nm for a doping concentration $\sim 10^{18} cm^{-3}$[29] and is assumed to be distributed equally between the n- and p- region. This calculated value is lower than the limit obtained with the model ($<3 \times 10^{15} cm^{-3}$). Hence, the simulated condition to achieve high efficiency gain factor is once again to be expected.

The likely occurrence of conditions assumed in the simulation has been justified. However, considering the midgap state as the only recombination center, will render the modeling versatility low. Various impurities at different concentrations and trap states exist in industry. Defects and interaction of these defects with impurities during a commercial fabrication process will further obscure the situation. Hence, the efficiency gain indicated by the simulation might not scale linearly upon application to industrial conditions.

It is, however, important to emphasize that the radial p-n junction nanorod solar cell design discussed above is not restricted to silicon only. In addition to silicon, simulations have been done for GaAs, with the result being a less dramatic improvement in efficiency due to the different length scales of the optical thickness (891nm for GaAs as compared to 125μm for Si). However, similar trends for J_{sc} and V_{oc} as those in silicon have also been observed. This shows that the improved efficiency offered by this design can also be

implemented with other semiconductor materials, as long as the two main conditions mentioned above are satisfied. This makes the designed structure really robust.

3.5.2 Nanorod Dye Sensitized Solar Cells

In principle, a substantial increase in DSC efficiency is attainable either by improving V_{oc}, J_{sc} or both of them simultaneously. V_{oc} is determined by the energy difference between the quasi-Fermi level of electrons within the oxide (TiO_2) film and the Fermi level of the redox couple. The option of increasing V_{oc} gives only a small efficiency payoff.

The option of improving J_{sc} is more promising. In principle, the maximum J_{sc} of a DSC is determined by how well the dye absorption window overlaps the solar spectrum. Hence, one way to enhance J_{sc} with the greatest potential to boost overall performance is to employ a new sensitizer with a higher molar extinction coefficient and broader spectral response than existing dyes. Approximately 85% of the total photon flux from the sun is between 300 nm and 1,400 nm. Thus by extending the absorption further more into NIR region, solar radiation can be more fully utilized. However, considerable efforts made to develop such dyes and dye mixtures that absorb better at long wavelengths have so far met with little success.

Another option to increase J_{sc} is to maximize red light conversion. Thickening the nanoparticle film to heighten the absorption of red and near-infrared light is nevertheless unsuccessful because the film thickness comes to exceed the electron diffusion length through the nanoparticle network. Another way is increasing the diffusion length of electrons within the nanocrystalline oxide, Ln, relative to the thickness of the oxide film, d, such that Ln/d $\gg$1 and d $>$ α^{-1}, where α is the wavelength-dependent absorption coefficient of the sensitized film.

Cell photocurrent is maximized if $L \gg d > \alpha^{-1}$ for all absorbed wavelengths because light harvesting and carrier collection are then very efficient. One promising solution to this is to increase the electron diffusion length in the anode by replacing the nanoparticle film

50

with an array of oriented single-crystalline nanowires. Electron transport (D_n) in crystalline wires is expected to be several orders of magnitude faster than percolation through a random polycrystalline network. Moreover, the rapid transport provided by a nanowire anode would be particularly favorable for cell designs that use non-standard electrolytes, such as polymer gels or solid inorganic phases, in which recombination rates are high compared with the liquid electrolyte cell.

A study by *Law et al*[9] has shown that electron diffusivity obtained in ZnO nanowire structures was several hundred to a thousand times faster that the highest reported diffusivity for TiO_2 or ZnO nanoparticle films in DSCs. This improvement in charge transport will contribute to the increase in J_{sc} (Figure. 28), and therefore efficiency. However, it has also been found that the overall performance is still limited by the dye loading. The longest arrays presented (20–25 μm), with diameter ranging from 130-200nm, can only provide one-fifth the active surface area of a nanoparticle anode.

Therefore, attaining a superior short-circuit current density (J_{sc}) with a nanowire cell of large L_n depends on fabricating single-crystalline nanowire arrays with surface areas at least as large as typical nanocrystalline films, which is a significant challenge. Using a sufficiently dense array of long, thin nanowires as a dye scaffold, it should be possible to increase the DSC dye loading (and so its absorption of red light) while simultaneously maintaining very efficient carrier collection.
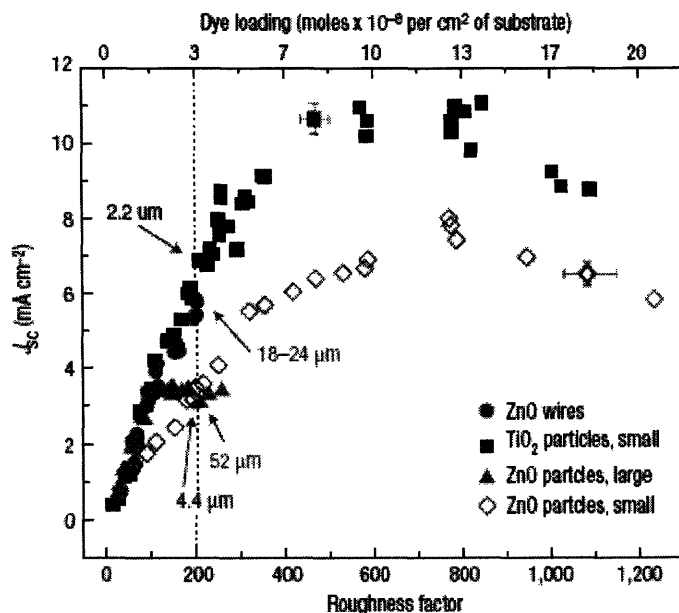
Figure 28. Comparative performance of nanowire and nanoparticle cells. Shortcircuit current density versus roughness factor for cells based on ZnO wires, small TiO$_2$ particles, and large and small ZnO particles. The TiO$_2$ films show a higher maximum current than either of the ZnO films, and a larger initial slope than the small ZnO particles, consistent with better transport through TiO$_2$ particle networks. The large ZnO particle cells attain a smaller maximum current than the small particles because the film thickness (and therefore the electron escape length) becomes larger than the electron diffusion length at a much lower roughness factor. The wire data fall on the TiO$_2$ line and significantly exceed the current output from both types of ZnO particle cells above a roughness factor of ~100. Cell thickness is directly proportional to roughness factor. [9]

Other attempts at increasing L_n, which depends on the electron diffusivity D_n and the electron lifetime τ_n according to $L_n = \sqrt{D_n \tau_n}$, have focused on slowing interfacial recombination (i.e., increasing τ_n) by adding surface coatings to the nanocrystalline film or speeding up electron transport (i.e., increasing D_n) by replacing TiO$_2$ with a different oxide in which electrons move faster. The latter approach however fails, apparently because electron diffusion within the nanocrystalline film is the rate-limiting step in the recombination process, making $D_n \propto \tau_n^{-1}$ and negating any positive impact of faster electron motion. Faster transport can be expected to improve DSC efficiency only when it does not trigger proportionally faster recombination.

Another study done by **Law et al** [30] has shown that carrier recombination in ZnO nanowire dye-sensitized cells can be suppressed by coating the nanowires in a conformal metal oxide shell made by atomic layer deposition (ALD). Applying the core-shell

concept to a nanowire photoelectrode provides a means to increase τ_n and L_n by augmenting the radial surface field that reflects electrons from the nanowire electrolyte interface. Recombination may remain diffusion limited, but the rate at which electrons sample the oxide surface is determined by the magnitude of the surface field rather than the diffusion constant for electrons in the wire cores. Diffusion lengths substantially larger than those of nanocrystalline films are therefore possible.

In principle, an oxide shell can suppress recombination by (i) introducing an energy barrier that increases the physical separation between photoinjected electrons and the oxidized redox species in the electrolyte, (ii) forming a tunneling barrier that corrals electrons within the conducting cores of the nanoparticle film, or (iii) passivating recombination centers on the oxide surface. Whether J_{sc} and cell efficiency improve also depends on the extent to which the electron injection and collection yields are hurt by the oxide shell. Hence, there exists an optimum coating thickness in which efficiency gain can be obtained by improved J_{sc}.

It is clear that by adopting nanorod structures, improved conversion efficiency can be achieved, as seen in simulations of radial p-n junction nanorod silicon solar cells and as seen in experiments on nanowire DSCs. Better electron transport in these nanorods/wires is a product of their excellent crystallinity and a radial electric field within each nanorod/wire that assists carrier collection by repelling photoinjected electrons from the surrounding electrolyte or providing shorter exciton diffusion lengths in DSC and silicon-based solar cells respectively.

4. Performance and Cost Analysis

Despite improvements in solar cell performance from the technological side, the costs needed for these improvements might not be economically practical. Hence, a cost analysis is done with some simplifying assumptions. A packing density of 100% is assumed in the simulation. Hence, it is assumed that no detrimental nor synergistic interaction between the two adjacent nanorods.

Satisfying the condition of low trap density at the depletion region, simulation of radial p-n junction nanorod cells has shown their superior performance (conversion efficiency) compared to planar cells. As simulated, this efficiency gain factor can vary from three to seven, depending on the minority carrier diffusion length, which, in turn, might depend on the impurities, defects and/or doping concentration. Carrier collection is enchanced only when $R < L_n$. Once R exceeds L_n, there will be a significant decline in carrier collection. Hence for modelling purposes, nanorods with radii of 100nm were used. This corresponds to the smallest L_n simulated.

Taking the efficiency of the radial solar cells to be five times that of planar solar cells and using a square pattern, calculation shows that for 200 nm diameter rods with a pitch of ~450 nm, a radial structure will no longer have an efficiency gain over planar structures. This value is however obtained by totally neglecting the contribution from the spacing area in which no nanorods are grown. With the current nanostructure processing technique capabilities to produce small spacings between nanostructures (high resolution), efficiency gain is hence certainly realizable.

A simple semi-quantitative cost analysis was done, based on the most important processes to realize both planar and nanorod solar cells. This involves purchasing wafers, doping through diffusion for planar solar cells. Although real devices, not even the prototypes, based on the radial solar cell design have not been built, likely processing steps were chosen and simplifying assumptions were made for this cost analysis. The manufacturing process (Figure. 29) starts with patterning arrays of metal catalyst though use of porous alumina templates, followed by electrodeposition of In catalysts and Si nanorod growth by the VLS method. The template would then be dissolved and diffusion will be used to dope the resulting nanorods to form p-n junction. Material and method of contacts formation is not discussed in this report, electrodes for contacts are hence excluded from this cost analysis.

54
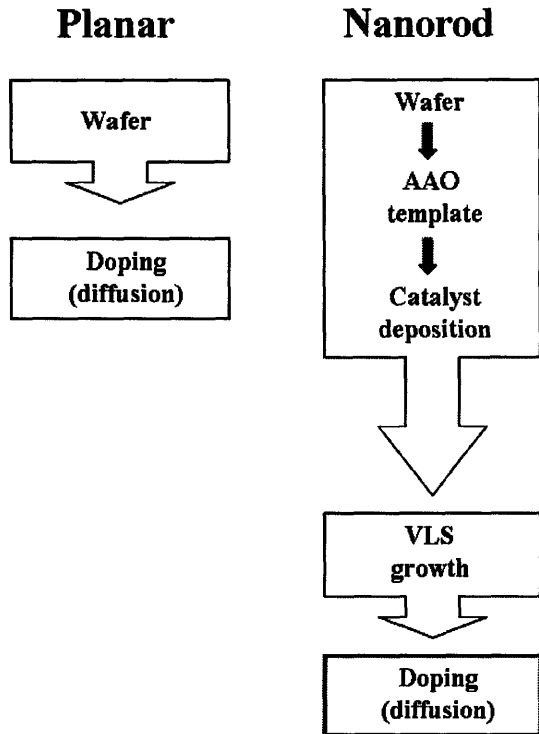
Planar   **Nanorod**

Figure 29. Process steps involved in fabricating planar and nanorod structure

As can be seen, realization of nanorod solar cells involves more steps than conventional planar cells. It is also apparent that there will be additional costs for every additional processing step taken. The main purpose for this cost analysis is to compare the increased in cost relative to the gain in efficiency for the nanorod solar cells discussed above, using conventional planar silicon solar cells as a reference.

The cost modeling process[*] showed that with the radial geometry and spacing designed for having efficiency twice that of planar structure (Diameter = 200nm and spacing = 100nm), it requires a manufacturing cost of 2.5 times that of planar cells. As far as "cost per watt PV-generated electricity" concern, this will result in relatively same value.

---

[*] **Price References**

1. http://beta.vwrsp.com/psearch/ControllerServlet.do?showallsuppliers=1&N=2757 &cntry=us&custpartgrp=null
2. https://www.siliconquest.com/store/index.php?click=|0|2&shopper=1178907493
3. http://www.sigmaaldrich.com/Area_of_Interest/The_Americas/United_States.html
4. http://www.caeonline.com/forsale.html
5. http://www.tedpella.com/gold_html/NanoParts.htm

However, most of this cost in this cost comes from labor and fixed cost (~80%). Hence, once an integrated manufacturing process was found, the cost can be further reduced while securing efficiency gain. Increasing the production capacity will further help in reducing the fixed cost contribution. No cost modeling is done on nanorod DSCs, given the absence of an exact quantitative analysis of potential efficiency improvements offered by employing the nanorod structure.

5. Market Analysis

The market analysis will be focused more on silicon-based solar cells, as they are much more established. However, some DSC companies have recently emerged. This shows the increasing importance of this type of solar cell. Being a unique market where there are a lot of government interventions, government-centric types of analysis can hence be applied to both types of solar cells.

5.1 Potential Sector of Initial Target Market

The solar cell market is subdivided into several application categories, namely on-grid residential, off-grid solar application, space solar, and the portable solar power market. The off-grid solar market, which involves uses such as billboard illumination and provision of electrical power in remote areas was ruled out due to small market share and no driving force for higher efficiency as in remote applications, space is not an issue. The portable solar market, which involves solar cells in portable devices, is also ruled out as an initial target market because the high focus on cost places radial p-n junction nanorod solar cell technology at a significant disadvantage compared to existing solutions.

The space solar market might also be excluded because of the high probability that the resulting efficiency from the structure might not be as good as technologies currently used. For comparison purposes, multijunction (3J or 4J) or tandem solar cells[31] have efficiencies much greater than other solar cell structure, including nanorod-based cells. The space solar market is anomalous because it has less sensitivity towards price. A

higher price is acceptable given the guaranteed higher performance gain (high efficiency coupled with lesser weight, and high resistance to the harsh environment conditions spacecraft are subjected to).

Therefore by elimination, on-grid residential application is the only potential initial target market. This includes the public utilities and commercial usage. The introduction of this new nanorod solar cell gives a substantial increase in the conversion efficiency albeit at reasonable higher initial cost.

5.2 Current Market Overview

The worldwide market for residential PV currently stands at approximately 10.6 billion US dollars in 2006, and is dominated by several countries, China, Japan, US and countries within the European Union. Around the world, governments are the main pushers for increased dependence on solar power. Through the introduction of various laws regarding the use of renewable energy, promoting continued research into green technologies and also providing subsidies for companies as well as the end consumers, governments play a major role in market creation

To illustrate the effect that various government policies have on market creation in different countries, brief summaries are given below. Government policies that regulate different markets must be considered because they affect not only the continued consumer interest in PV, but also in the provision of susbsidies and incentives which may make an otherwise unprofitable enterprise lucrative.

5.2.1 Japan

Multi crystalline silicon and single crystalline silicon solar cell and module technologies have dominated the Japanese PV market with a share of about 95%.[32] Japanese PV production, which accounts for 49% of the world total, has benefited from a variety of government incentive programs. The 70,000 Roofs Program established in 1994 initially covered 50 percent of PV installation costs. As the cost of solar cells fell with increased

production, however, the subsidy was reduced to about 10 percent. By 2002, the number of residential systems installed in Japan had reached 144,000.

Other useful government incentives include a budget allocation of 20.5 billion yen ($186 million) in 2003 for research and development, demonstration programs, and market incentives and net-metering (feeding excess energy back into the power grid). Within nine years, from 1994 to 2003, these programs helped Japan position itself as the world leader in both production and installation of solar cells.

5.2.2 European Union (EU)

European production has boomed. With a growth of 41% in 2003, PV production in Europe reached 190 MW. Despite the lack of a unified EU approach toward renewable energy, individual member states' policies have enhanced Europe's position in the world market.

Germany, positioned itself with the 100,000 Roofs Program, launched in late 1998, which provided 10-year low-interest loans for PV installation (it ended early, in 2003, when all targets were met). Germany now leads the way with an Electricity Feed-in Law that started in 1999, which permits most customer applications to receive 45.7 euro cents per kilowatt-hour (kWh) (56¢ per kWh) for solar-generated electricity sold back to the grid. By the end of 2003, German installed capacity was 400 MW, well beyond the initial goal of 300 MW. The rising number of market implementation programs, as well as various regional incentive programs, provides a bright outlook for the solar industry both in Germany and in Europe as a whole.

In 2004, the German government introduced the first large scale feed in tariff (FIT) system, which resulted in explosive growth of PV installations in Germany. Feed-in tariff term usually refers to the regulatory, minimum guaranteed price per kWh that an electricity utility has to pay to a private, independent producer of renewable power fed into the grid. The principle behind the German system is a 20 years flat rate contract. The value of new contracts is programmed to decrease each year, in order to encourage the industry to pass on lower costs to the end users.

With the above mentioned government support, Germany strengthened its position as the leading national solar photovoltaic (PV) market in 2005 with growth of 53% to 837 Megawatts of newly installed capacity, according to the new "German PV Market Report 2006" issued by San Francisco based PV consultancy, Solarbuzz LLC. Of the 837 Megawatts, 7 Megawatts are accounted for by off-grid systems, while the grid connect market accounted for 830 Megawatts. Residential customers continue to underpin the German PV market. They accounted for 40% of new installations in 2005. The next largest segment of agricultural customers represented 28% of the market.

Subsequently Spain, Italy, Greece and France introduced feed-in tariffs. None have replicated the programmed decrease of FIT in new contracts though, making the German incentive relatively less and less attractive compared to other countries. The French FIT offers a uniquely high premium for building integrated systems.[33]

5.2.3 Unites States (US)

In contrast, the United States government is not as active in promoting PV usage as Japan or Germany. However, success achieved mainly by these two countries has triggered the US to be more attentive to this issue (Figure. 30). Hence, government support and funding that flows into the PV research area has started to increase.
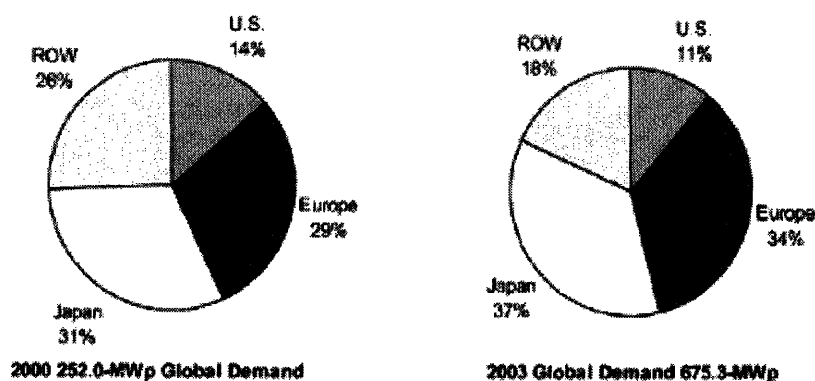

Figure 30: Regional solar-cell market shares in 2000 and 2003. ROW refers to the rest of the world.[34]

President Bush's Solar America Initiative (SAI) is a commitment to diversify energy resources through grants, incentives and tax credits. It aims to spur widespread

commercialization and deployment of clean solar energy technologies across America, which would provide long-term economic, environmental, and security benefit to the nation. The SAI is also a key component of President Bush's Advanced Energy Initiative, which provides a 22% increase in research and development funding at the Department of Energy (DOE) and seeks to reduce the dependence on foreign sources of oil.

In March 2007, DOE selected 13 solar energy projects for up to $168 Million in funding. These projects were distributed to 13 solar cell companies: Amonix, Boeing, BP Solar, Dow Chemical, General Electric, Greenray, Konarka, Miasole, Nanosolar, Powerlight, Practical Instruments, SunPower and United Solar Ovonic. This is the first funding awards for Solar America Initiative to make solar technology cost-competitive by 2015[35]. This supports will enable the projected expansion of the annual US manufacturing capacity of PV systems from 240 MW in 2005 to as much as 2,850 MW by 2010, representing more than a ten-fold increase.

There were significant shifts in the share of the five main end-market segments, as the large commercial segment grew fastest to reach 33% of the total grid connect market. In terms of application surface, the largest share was held by commercial flat roofs, which accounted for 23% of the market. [36]

5.2.4 China

The last market considered is that of China. Although the market is currently small (4.25MW in 2002), growth is expected to be drastic as China's electricity consumption: nearly triples over the next two decades, growing by an average annual rate of 4.3%. A national goal to supply 10% of the total primary energy in 2020 with renewable energy has been set and a commitment of 2008 Peking to be a "Green Olympics". [37] China may therefore soon become an important player in this field. According to officials, the government is ready to invest $1.2 billion in solar energy development over the next five years.

5.2.5 Overall Financial Incentives Assessment

The political purpose of incentive policies for PV is to grow the industry even where the cost of PV is significantly above grid parity*, to allow it to achieve the economies of scale necessary to reach grid parity. The policies are implemented to promote national energy independence and reduction of CO_2 emissions.

Incentive mechanisms generally implemented (might be in combination)[38] include:

- Investment subsidies: the authorities refund part of the cost of installation of the system
- Feed-in tariffs (FIT)/net metering: the electricity utility buys PV electricity from the producer under a multiyear contract at a guaranteed rate
- Renewable Energy Certificates (RECs)

With investment subsidies, the financial burden falls upon the taxpayer, while with feed-in tariffs the extra cost is distributed across the utilities customer base. While the investment subsidy may be simpler to administer, the main argument in favour of feed-in tariffs is the encouragement of quality. Investment subsidies are paid out as a function of the declared capacity of the installed system and are independent of its actual power yield over time, thus rewarding the overstatement of power and tolerating poor durability and maintenance.

With feed-in tariffs, the financial burden falls upon the consumer. They reward the number of kilowatt-hours produced over a long period of time, but because the rate is set by the authorities, it may result in perceived overpayment. The price paid per kWh under a feed-in tariff exceeds the price of grid electricity. "Net metering" refers to the case where the price paid by the utility is the same as the price charged.

Feed-in tariffs may be based on either the so-called 'avoided costs' of non-renewable power producers or the electricity price charged to the end-user, supplemented by a bonus or premium in order to account for the social or environmental benefits of renewable electricity. On the other hand, feed-in tariffs may also be fixed at a certain level just to

---

* Grid parity is the point at which photovoltaic electricity is equal to or cheaper than grid power.

encourage the generation of renewable electricity without any direct relation to the costs or price of non-renewable power production.

Where price setting by supply and demand is preferred, renewable energy certificates (RECs) can also be used. In this mechanism, a renewable energy production or consumption target is set, and the consumer or producer is obliged to purchase renewable energy from whoever provides it the most competitively. The producer is paid via an REC. In principle this system delivers the cheapest renewable energy, since the lowest bidder will win. However uncertainties about the future value of energy produced are a major hindrance to investment in capacity, and the higher risk increases the cost of capital borrowed. Hence, though this system really encourages competition in cost and efficiency of the cell, the number of companies that are willing to bear such high risk to start with is low.

On the other hand, though feed-in tariffs may be set at a uniform level, they are often differentiated depending on other variables such at the time or season of feeding renewable energy into the grid. In addition, the system of determining feed-in tariffs may be either fixed for a certain, multi-annual period (in order to provide renewable energy producers certainty in the medium or long term) or adjusted periodically in order to maintain some flexibility and to account for unforeseen cost reductions of renewable power production. Finally, the level and importance of feed-in tariffs may vary significantly among countries, depending on national characteristics such as the potential and costs of renewable resources or the political preferences regarding policy instruments to promote renewable electricity.

Given all the flexibilities for modifications, it may be concluded that a system of premium feed-in tariffs has shown to be an effective instrument to promote the generation of renewable electricity, notably to ensure a low-level market take-off of solar power at the national level. In the longer term, however, such a system may become hard to sustain as it may suffer from some major drawbacks, especially when the generation of green electricity accounts for a significant share in total power production.

These disadvantages refer particularly to the fact that a system of fixed premium prices tends to be costly, inefficient, and distortive of competitive pricing. In the long run, the best way to encourage renewable electricity is probably either to internalise the external costs and disadvantages of non-renewable energy sources (e.g. by means of taxation) or to introduce market-conform instruments such as a well-functioning system of tradable green certificates (where the price of these certificates accounts for the social and environmental benefits of renewables compared to non-renewables). However, it may take quite some time – if ever – before either one of these 'best means' (or a combination of both) will be achieved. In the meantime, feed-in tariffs can and will be justified in as the best alternative instrument to encourage the generation of a certain amount of green electricity, notably when this amount is still small.

5.3 2007 World Photovoltaic Industry Report Highlights [39]

World solar PV market installations reached a record high of 1,744 megawatts (MW) in 2006, representing growth of 19% over the previous year.
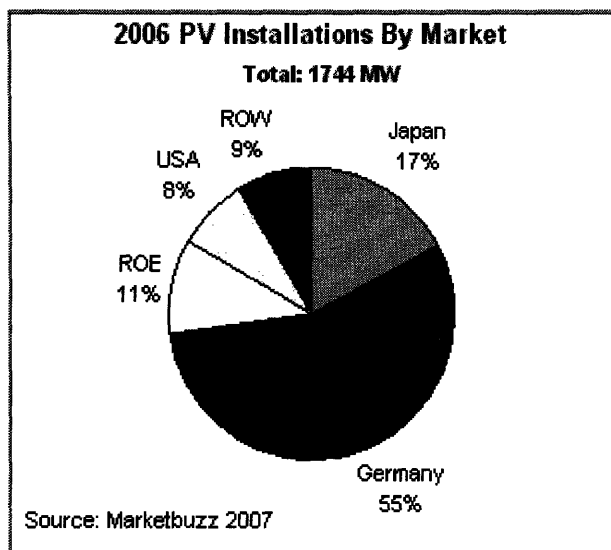

Figure 31. Breakdown chart of PV installation market on 2006[39]

Germany's grid connect PV market grew 16% to 960 Megawatts in 2006 and now accounts for 55% of the world market. While Japan's market size barely advanced last year, Spain and the United States were the strong current performers. The Spanish market was up over 200% in 2006, while the US market grew 33%.

World solar cell production reached a consolidated figure of 2,204 MW in 2006, up from 1,656 MW a year earlier. Japanese producers lost ground over the past 12 months, dropping from 46% to 39% share, to the benefit of Chinese cell manufacturers. Global industry revenues were $10.6bn in 2006, while capital investment through the PV business chain totaled $2.8bn. The industry raised over $4bn in equity and debt financing, up from $1.8bn the previous year. This review gives insight into the size of the industry and once again emphasizes significant government's role in market creation. As can be seen, Japan and Germany (the two pioneer countries that depicts the success of government's initiative in solar cell development), have now become the two countries with major market share as well as manufacturing players.

5.4 Deductive Market Reasoning

The grid-connected market remains the major trophy for the solar industry, because of the huge scale of the electricity supply market (Table. 6). Indeed, this is where growth has been strongest recently. While solar is a long way from competing with conventional power generation costs at 3-5 cents/kWh, it is much closer to reaching electricity tariffs charged to residential, commercial and industrial consumers. This is especially relevant because when the PV is sited at the consumers premises, then the comparison for the customer is between the tariff rate and the cost of PV electricity from his system.

Precise calculation of solar electricity costs depend on the location and the cost of finance available to the owner of the solar installation, but with the best PV electricity prices (in the sunniest locations) approaching 30 cents/kWh and the highest tariffs now exceeding 20 cents/kWh, the gap is now relatively narrow. Funding programs that bridge this gap are causing rapid growth in sales of solar PV, especially in Japan and Germany. Analysts note that for every cumulative doubling in PV production, there is a 20% decline in costs. With an annual average growth rate of over 30% since 1995, this translates into a 5% cost reduction per year.

64

	Solar markets (av of large 5 years)	Solar Price/Competing Energy source
Remote Industrial	17%	0.1-0.5 times
Remote Habitational	22%	0.2-0.8 times
Grid Connected	59%	2-5 times
Consumer Indoor	2%	n/a

Table 6. Solar market sector breakdown[40]

An analysis of electricity rates around the world, shows that the solar industry is rapidly approaching the point where commercial on-grid market niches will be created in selected countries or regions where electricity rates are high (Table. 7). The pattern of changes in the market have been underpinned by differences in investment economics for PV in each customer segment and this fast changing picture is a key element of how the market will evolve over the next two years.

Country	Cents/kWh
Argentina	14.1
Australia	8*
Austria	16.8*
Belgium	16.5**
Brazil	12.8**
Denmark	20.7
France	12.9**
Germany	15.2
India	3.4*
Indonesia	2.5
Japan	21.2
Mexico	5.9
Netherlands	13.2
Portugal	14.1
Spain	14.3
Switzerland	13.1
United Kingdom	11.7
United States	8.1

Table 7. Residential electricity tariffs in 1999[41]

The going trend (1999-2006) of on-grid residential application as the major sector of solar market coupled with several available potential commercial niches for the solar market (countries with relatively high electricity tariffs), there will be short-run market available for solar cell to penetrate and survive.

Successful market creation using the FIT system has been seen in several countries (e.g., Germany, French and Spain). Combined FIT with REC system might be the most beneficial projected method for market creation and sustenance, respectively. Using the REC system in the long run will help in promoting competitive action between the solar cell producers in utilizing cells with increasing efficiency at economically additional cost. Substantial support from these proven successful stories of government interference in creating markets in Germany and Japan, together with the anticipated long run plan, might also help induce government involvement in other countries. With more government supports in different countries, prices for solar cells can be further reduced. This price reduction coupled with increasing worldwide concern about clean renewable energy will allow developing countries to be targeted as a huge next-generation potential market. In this way, developing countries, in addition to developed countries, can be involved in the usage of solar cells.

6. Conclusion and Future Recommendations

Simulation or experiment have successfully shown that superior performance in existing solar cell designs is achieved through the incorporation of nanorod structures. Harnessing the main nanorods feature of having much higher carrier mobilities for better electron transport, improvement in either J_{sc} or V_{oc} has been observed in nanorod DSCs as well as nanorod-silicon-based solar cell.

Better electron transport in these nanorods/wires is a product of their excellent crystallinity and a radial electric field within each nanorod/wire that assists carrier collection by repelling photoinjected electrons from the surrounding electrolyte and providing shorter exciton diffusion lengths in DSCs and silicon-based solar cells,

respectively. The properties of nanorods are in fact highly dependent on the fabrication process used. Combination of the AAO templating method with the VLS growth process was chosen to ensure control over the physical dimension of the resulting nanorods and their crystallinity, respectively. Radial p-n junction silicon-based solar cells offers efficiency gain over planar cells, with a reasonable increase in cost, based on the simplified cost modeling described before.

Having both the technological advantages with reasonable cost increment and huge potential market as explained before, the commercialization process of this nanorod-designed solar cell looks favorable. Furthermore, being a silicon-based technology; this design will encounter less resistance upon incorporation into an existing industry familiar with silicon processing techniques. However, the incorporation of this nanorod structure into silicon based PV cell must be brought into product actualization as soon as possible, when silicon-based PV systems are still occupying majority of the market.

An actual prototype of a radial p-n junction nanorod solar cell has not successfully been constructed or tested yet. This report has so far concentrated on the properties of nanorods themselves. Problems arising from their processing and integration have not been fully addressed and solved yet. Thus, further investigation into the materials used for electrodes or contacts and methods for forming contacts will be beneficial, since it will give an even more complete picture. The possibility of having synergistic effects of dye-sensitized silicon nanorod solar cells is also worth being explored more intensively. In this report, attempts done so far by exploring and comparing the mechanism of both types of solar cells have shown no opposing sign. Even so, further study into the surface chemistry of the semiconductor material, the dye used and reaction involved between the electrolyte with the dye as well as with the semiconductor material will be highly useful.

7. References

1. Gratzel, M. (2001). Photoelectrochemical Cells. Nature, 414, 338-344.

2. Kayes, B.M., Spurgeon, J.M., Sadler, T.C., Lewis, N.S., & Atwater, H.A. (2006). Synthesis and Characterization of Silicon Nanorod Arrays for Solar Cell Applications. IEEE 4th World Conference on Photovoltaic Energy Conversion Proceedings.

3. Wagner, R.S., & Ellis, W.C. (1964). Vapor-Liquid-Solid Mechanism of Single Crystal Growth. Applied Physics Letters, 4, 89-90.

4. Law, M., Goldberger, J., & Yang, P. (2004). Semiconductor Nanowires and Nanotubes. Annu. Rev. Mater. Res., 34, 83-122.

5. Civale, Y., Nanver, L.K., Hadley, P., & Goudena, E.J.G. Aspects of Silicon Nanowire Synthesis by Aluminum-Catalyzed Vapor-Liquid-Solid Mechanism, http://med.tn.tudelft.nl/~hadley/publications/safe/civale-safe2004.pdf

6. Kamins, T.I., & Williams, R.S. (2001). Ti-Catalyzed Si Nanowires by Chemical Vapor Deposition: Microscopy and Growth Mechanism. Journal of Applied Physics, 89, 1008-1016.

7. Huang, M.H. et al. (2001). Room-Temperature Ultraviolet Nanowire Nanolasers. Science, 292, 1897-1899.

8. Huang, M.H., Wu, Y., Feick, H., Tran, N., Weber, E., & Yang, P. (2001). Catalytic Growth of Zinc Oxide Nanowires by Vapor Transport. Advanced Materials, 13, 113-116.

9. Law, M., Greene, L.E., Johnson, J.C., Saykally, R., & Yang, P. (2005). Nanowire Dye-Sensitized Solar Cells. Nature Materials, 4, 455-459.

10. Shimizu, T., Xie, T., Nishikawa, J., Shingubara, S., Senz, S., & Gosele, U. (2007). Synthesis of Vertical High-Density Epitaxial Si(100) Nanowire Arrays on a Si(100) Substrate Using an Anodic Aluminum Oxide Template. Advanced Materials, 19, 917-920.

11. Hochbaum, A.I., Fan, R., He, R., & Yang, P. (2005). Controlled Growth of Si Nanowire Arrays for Device Integration. Nano Letters, 5, 3, 457-460.

12. http://en.wikipedia.org/wiki/Solar_cell

13. Wadell, A.L., & Forrest, S.R. High Power Organic Solar Cells from Efficient Utilization of Near-Infrared Solar Energy. Green Power Magazine

14. Bailey, S.G., Castro, S.L., Raffaelle, R.P., Fahey, S., Gennett, T., & Tin, P. (2003). Nanostructured Materials for Solar Cells. 3rd World Conference on Photovoltaic Energy Conversion

15. Honsberg, C.B., Barnett, A.M., & Kirkpatrick, D. (2006). Nanostructured Solar Cells for High Efficiency Photovoltaics. IEEE, 2565-2568

16. http://www.solarserver.de/wissen/photovoltaik-e.html

17. Sopori, B. (2002). Silicon Solar-Cell Processing for Minimizing the Influence of Impurities and Defects. Journal of Electronic Materials, 31, 972-980.

18. Nelson, J. (2002). Organic Photovoltaic Films. Solid State and Materials Science, 6, 87-95.

19. Kannan, B., Castelino, K., & Majumdar, A. (2003). Design of Nanostructured Heterojunction Polymer Photovoltaic Devices. Nano Letters, 3, 1729-1733.

20. Milliron, D.J., Gur, I., & Alivisatos, A.P. (2005). MRS Bulletin, 30.

21. Huynh, W.U., Dittmer, J.J., & Alivisatos, A.P. (2002). Hybrid Nanorod-Polymer Solar Cells. Science, 295, 2425-2427.

22. Gur, I., Fromer, N.A., Geier, M.L., & Alivisatos, A.P. (2005). Air-Stable All-Inorganic Nanocrystal Solar Cells Processed from Solution. Science, 310, 462-464

23. Gratzel, M. (2005) Energy Conversion by Dye-Sensitized Photovoltaic Cells. Inorganic Chemistry, 44, 6841-6851.

24. Kayes, B.M., & Atwater, H.A. Comparison of the Device Physics Principles of Planar and Radial p-n Junction Nanorod Solar Cells. (2005). J. Appl. Phys, 97, 114302.

25. Schlosser, V. (1984). Limiting Factors for the Application of Crystalline Upgraded Metallurgical Grade Silicon. IEEE Transactions on Electronic Devices, 31,610-613.

26. http://www-als.lbl.gov/als/science/sci_archive/112solarcells.html, http://www.aps.anl.gov/News/Meetings/Monthly_Meetings/2005/Presentations/20 050914_BLai.pdf

27. http://en.wikipedia.org/wiki/Semiconductor

28. Kim, J.K., Anderson, W.A., & Hyland, S.L. (1978). Interface State Measurements and Computer Simulation Studies of MIS Solar Cells. Electronic Devices Meeting, 24, 90-92.

29. Pierret, R.F. (1996). Semiconductor Device Fundamentals. Addison-Wesley, p.218.

30. Law, M., Greene, L.E., Johnson, Radenovic, A., Kuykendall, T., Liphardt, J., & Yang, P. (2065). ZnO-Al$_2$O$_3$ and ZnO-TiO$_2$ Core-Shell Nanowire Dye-Sensitized Solar Cell. J.Phys.Chem.B, 110,22652-22663.

31. Tanabe, K., Morral. A.F., & Atwater, H.A.(2006). Direct-Bonded GaAs/InGaAs Tandem Solar Cell. Applied Physics Letters, 89, 102106.

32. Yamaguchi, M., Ohshita, Y., Arafune, K., Sai, H., & Tachibana, M. (2006). Present Status and Future of Crystalline Silicon Solar Cells in Japan. Solar Energy, 80, 104-110.

33. http://www.solarserver.de/solarmagazin/index-e.html

34. Mints, P. (2006). PV-The Story So Far. Refocus, 7, 32-36.

35. http://www.energy.gov/news/4855.htm

36. http://solarbuzz.com/USGridConnect2006.htm

37. Yang, H., Wang, H., Yu, H., Xi, J., Cui, R., & Chen, G. (2003). Status of Photovoltaic Industry in China. Energy Policy, 31, 703-707.

38. http://en.wikipedia.org/wiki/Photovoltaic

39. http://www.solarbuzz.com/Marketbuzz2007-intro.htm

40. http://solarbuzz.com/StatsCosts.htm

41. Wu, Y., Yan, H., & Yang, P. (2002). Semiconductor Nanowire Array: Potential Substrates for Photocatalysis and Photovoltaics. Topics in Catalysis, 19,197-202.